Physical Amplification of Chemical Colorimetric Sensing and a Transfer Matrix Analysis

Keegan Quigley
Advisor: Dr. Jimmy Xu

A thesis presented for the degree of
Bachelor of Science, Engineering Physics

Department of Physics
Brown University
May 3, 2018

Abstract

The development of the Transfer Matrix Method for electromagnetic and acoustic wave propagation through multi-layered material proves useful for quantitative design, optimization, and analysis of photonic and acoustic devices. Its utility is demonstrated in the exploration of structural coloration in colorimetric sensing, in which we use the Transfer Matrix Method to simulate reflection spectra and color of a variety of color-changing material structures. With the introduction of metrics "color-distance" and "color-change amplification", we explore the role that physical structure can play in enhancing color-changes beyond what is currently achievable through chemical reactions. We show that using the methods outlined, physical amplification of color-change can lead to thinner reactive layers, thereby maximizing both response speed and sensitivity.

Acknowledgements

This thesis would not have been possible without the assistance and support from a number of people. I would like to thank my research group, the *Laboratory for Emerging Technologies*, under the lead of Dr. Jimmy Xu. Rachel Odessey and Dr. Do-Joong Lee were both immensely helpful in their expertise on the subjects of colorimetric sensing and chemistry. The external support for our lab from the Defense Threat Reduction Agency (DTRA) and US Army Natick Soldier Research Development and Engineering Center (NSRDEC) was critical in the development of the project and its continued success. Thank you to Dr. Richard Osgood of NSRDEC for his direct involvement on the project. I would also like to give a huge thank you to my family and friends who have supported me, both here at Brown and elsewhere.

Chapter 1

The Transfer Matrix Method (TMM)

The Transfer Matrix Method (TMM) is a computational method of describing the propagation of waves through multi-layered media. It has been used extensively in the study of optics, and can be used to study acoustics, as well. [1, 2, 3] The method uses a matrix to describe a stack of materials through which waves propagate, yielding a translation of fields from one side of the stack to the other. It provides a precise solution in cases where infinite internal reflections in the popular alternative ray-optics approach may make direct analytical solutions intractible.

Maxwell's equations dictate continuity conditions that help us understand how electromagnetic waves transform across boundaries in dielectric material. When incident light arrives at such a boundary, a portion of that light is reflected and a portion is transmitted. Fresnel's Equations, derived from Maxwell's Equations and boundary conditions, describe the reflection and transmission of electromagnetic waves across a layer boundary[4].

When light is incident on a multi-layered stack of dielectric materials with more than one boundary (Fig 1.1), the number of computations required to fully calculate the reflected and transmitted waves becomes infinite due to internal reflections. Furthermore, these reflections and transmissions between boundaries can lead to constructive or destructive interference of waves, depending on phase changes during wave propagation. While simple structures can be approximated with the use of Fresnel's Equations, keeping track of the phase of the wave and its reflections quickly becomes a challenging computational problem with any more than two boundaries.

The Transfer Matrix Method turns to matrix multiplication to solve this complex problem. It uses a single matrix to describe an entire dielectric stack in one matrix, allowing for a translation of forward and backward propagating electric field waves (E_+ and E_-, respectively) across the multi-layered dielectric material. The electric field at the left

boundary of the stack is denoted E whereas the electric field at the right boundary is denoted E'

$$\begin{bmatrix} E_+ \\ E_- \end{bmatrix} = T \begin{bmatrix} E'_+ \\ E'_- \end{bmatrix} \tag{1.1}$$

The transfer matrix T, describing the material and its effect on electric fields, multiplies the electric field vector describing the electric fields immediately to the right of the dielectric stack, to find the electric fields immediately to the left of the stack. This is how the transfer matrix will be set up for the remainder of the derivation. If we only consider reflections, the ratio of the two field components at the left boundary can be used to describe the reflected wave, with E'_- set to zero.

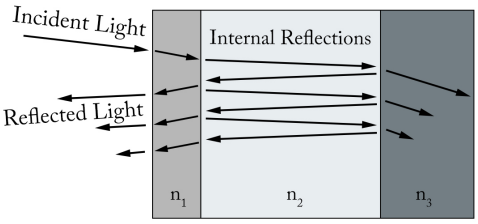

Figure 1.1: Internal reflections of incident light in layered media make calculations of reflected light difficult. The Transfer Matrix Method offers an elegant solution to the problem.

Although the traditional use of the TMM is for the analysis of electromagnetic wave reflections, the same method can be converted into use for acoustic waves. Acoustic waves satisfy mathematically similar wave equations, leading to similar boundary conditions and similar formulation of the transfer matrix. In the following, the TMM is re-derived, instead of adopted from literature, for the benefit of arriving at a more complete and detailed understanding and a self-contained reference.

1.1 Electromagnetic Transfer Matrix

1.1.1 Reflections at Boundaries (Fresnel's Equations)

The derivation of the transfer matrix method begins with the electromagnetic boundary conditions in the absence of free currents or charges.[4]

$$(i) \quad \epsilon_1 E_1^{\perp} = \epsilon_2 E_2^{\perp} \qquad (iii) \quad E_1^{\parallel} = E_2^{\parallel}$$

$$(ii) \quad B_1^{\perp} = B_2^{\perp} \qquad (iv) \quad \frac{1}{\mu_1} B_1^{\parallel} = \frac{1}{\mu_2} B_2^{\parallel}$$

These describe the relationship between electric and magnetic fields (both perpendicular ($\perp$) and parallel ($\parallel$) to the boundary) on either side of a boundary . Considering a monochromatic plane wave of angular frequency ω approaching the boundary from

the left with normal incidence (in the $\hat{z}$ direction), the incident (I) electric and magnetic field waves, at time $t = 0$, are given by

$$\tilde{E}_I(z,t) = \tilde{E}_I e^{i(k_I z - \omega t)} \qquad \tilde{B}_I(z,t) = \frac{k_I}{\omega}\tilde{E}_I e^{i(k_I z - \omega t)}$$

where $\tilde{E}$ indicates that E can contain both complex and real components, as it absorbs any initial phase ϕ as $\tilde{E} = Ee^{i\phi}$. $\tilde{B}_I(z,t)$ is derived from Faraday's Law, which states $\nabla \times \mathbf{E} = -\frac{\partial \mathbf{B}}{\partial t}$, or put to use here:

$$\tilde{\mathbf{B}} = \frac{k}{\omega}(\hat{z} \times \tilde{\mathbf{E}}) \tag{1.2}$$

This incident wave gives rise to reflected and transmitted waves at the boundary surface:

$$\tilde{E_R}(z,t) = \tilde{E_R} e^{i(k_R z - \omega t)} \qquad \tilde{B_R}(z,t) = \frac{k_R}{\omega}\tilde{E_R} e^{i(k_R z - \omega t)}$$

$$\tilde{E_T}(z,t) = \tilde{E_T} e^{i(k_T z - \omega t)} \qquad \tilde{B_T}(z,t) = \frac{k_T}{\omega}\tilde{E_T} e^{i(k_T z - \omega t)}$$

Recognizing that $k_R = -k_I$ (from Snell's Law), the boundary conditions (iii) and (iv) can now be used to relate the reflected and transmitted waves to the incident wave.[4] From (iii), which states that the parallel components of the electric field must be equal across the interface:

$$\tilde{E_I} + \tilde{E_R} = \tilde{E_T} \tag{1.3}$$

And from (iv):

$$\frac{k_I}{\mu_1 \omega}(\tilde{E_I} - \tilde{E_R}) = \frac{k_T}{\mu_2 \omega}\tilde{E_T} \tag{1.4}$$

Together, Equations (1.3) and (1.4) establish the relationships between E_I, E_R and E_T:

$$\frac{k_I}{\mu_1 \omega}(\tilde{E_I} - \tilde{E_R}) = \frac{k_T}{\mu_2 \omega}(\tilde{E_I} + \tilde{E_R}) \tag{1.5}$$

$$\frac{k_I}{\mu_1 \omega}(2\tilde{E_I} - \tilde{E_T}) = \frac{k_T}{\mu_2 \omega}\tilde{E_T} \tag{1.6}$$

We can simplify these equations by defining the *index of refraction*, $n = \frac{ck}{\omega}$, a property of the material through which the waves travel. The value of n has a dependence on frequency ω, and can be both real and complex valued, such that $\tilde{n}(\omega) = n(\omega) + i\kappa(\omega)$. For a monochromatic plane wave of frequency ω,

$$\frac{k}{\mu\omega} = \frac{\sqrt{\epsilon_0 \mu_0}}{\mu} n(\omega)$$

where $c = \frac{1}{\sqrt{\epsilon_0 \mu_0}}$, the speed of light in a vacuum. We can define

$$\beta = \frac{\mu_1 n_2}{\mu_2 n_1} \approx \frac{n_2}{n_1}$$

(as $\mu \approx \mu_0$ for most materials) to easily express the relationships between incident, reflected, and transmitted waves (Fresnel's Equations).

$$\tilde{E_R} = \Big(\frac{1-\beta}{1+\beta}\Big)\tilde{E_I} \tag{1.7}$$

$$\tilde{E_T} = \Big(\frac{2}{1+\beta}\Big)\tilde{E_I} \tag{1.8}$$

These relate the complex amplitudes of the electric fields on either side of the boundary during reflection and transmission.

The intensity of the fields can be derived from the time-averaged Poynting Vector S (which describes the energy traveling in an electromagnetic wave), and Equation (1.2):

$$I = |\mathbf{S}| = \frac{1}{\mu}(\mathbf{E} \times \mathbf{B}) = \frac{1}{2}\frac{\sqrt{\epsilon_0 \mu_0}}{\mu} n(\omega)|E|^2 \tag{1.9}$$

such that the reflection and transmission can be described in terms of their respective intensities (relative to the incident wave)

$$\frac{I_R}{I_I} = \Big(\frac{\tilde{E_R}}{\tilde{E_I}}\Big)^2 = \Big(\frac{1-\beta}{1+\beta}\Big)^2 \tag{1.10}$$

$$\frac{I_T}{I_I} \approx \frac{n_1}{n_2}\Big(\frac{\tilde{E_T}}{\tilde{E_I}}\Big)^2 = \frac{n_1}{n_2}\Big(\frac{2}{1+\beta}\Big)^2 \tag{1.11}$$

Eqn.(1.10) describes the intensity of a reflection. That is, the fraction of energy in an incident wave reflected at at the first boundary of the dielectric stack.

1.1.2 Multi-layered Material

To make the transfer matrix useful in calculating reflectance, we need to be able to derive a transfer matrix equation of the form:

$$\begin{bmatrix} E_+ \\ E_- \end{bmatrix} = T \begin{bmatrix} E'_+ \\ 0 \end{bmatrix}$$

This form is similar to Equation (1.1) with one minor difference: the backward traveling electric field on the right side (E'_-) of the last layer of the dielectric stack has been set to 0. This implies the physical equivalent of a multi-layered dielectric stack with light incident on only the left side. A transmission through the right boundary is possible

(E'_+), as well as a reflection off the left boundary, (E_-), but no backward traveling wave is incident on the stack. This allows for a measurement of the reflection coefficient Γ for an incident wave of any magnitude.

The Transfer Matrix must describe two processes: the reflection and transmission of waves at boundaries, and the propagation of waves through layers of the dielectric stack. To do this, the transfer matrix is broken into two types of matrices that can be multiplied together to describe the full dielectric stack. The first type of matrix derived will be a Propagation Matrix, denoted P, and the second will be a Boundary Matrix, denoted M.

Throughout the derivation, we describe the electric and magnetic fields as a superposition of waves traveling in the positive and negative $\hat{z}$ directions, previously called the forward and backward directions.

$$\tilde{E}(z,t) = \tilde{E}_+ e^{i(kz-\omega t)} + \tilde{E}_- e^{i(-kz-\omega t)} \tag{1.12}$$

$$\tilde{B}(z,t) = \frac{k}{\omega}[\tilde{E}_+ e^{i(kz-\omega t)} - \tilde{E}_- e^{i(kz-\omega t)}] \tag{1.13}$$

We only need to explore spatial dependence, however. At $t = 0$, (1.12) and (1.13) become:

$$\tilde{E}(z) = \tilde{E}_+ e^{ikz} + \tilde{E}_- e^{-ikz}$$

$$\tilde{B}(z) = \frac{k}{\omega}[\tilde{E}_+ e^{ikz} - \tilde{E}_- e^{-ikz}]$$

1.1.3 Propagation Matrix

The propagation matrix P is the way that we can model propagation of an electric field wave through a material of arbitrary thickness l. We can rewrite the expression of the superimposed forward and backward traveling waves (1.12) in matrix form:

$$\tilde{E}(z) = \begin{bmatrix} \tilde{E}_+(z) \\ \tilde{E}_-(z) \end{bmatrix}$$

In this expression, the phase has once again been absorbed into the complex valued $\tilde{E}$. These phases can also be described as

$$\tilde{E}_+(z) = \tilde{E}_+(0) e^{ikz}$$

$$\tilde{E}_-(z) = \tilde{E}_-(l) e^{ik(l-z)}$$

Focusing solely on the relative phases at either end of the layer, we can rewrite these relations in matrix form:

$$\tilde{E}(l) = \begin{bmatrix} \tilde{E}_+(l) \\ \tilde{E}_-(l) \end{bmatrix} = \begin{bmatrix} e^{ikl} & 0 \\ 0 & e^{-ikl} \end{bmatrix} \begin{bmatrix} \tilde{E}_+(0) \\ \tilde{E}_-(0) \end{bmatrix} \tag{1.14}$$

However, since the Transfer Matrix operates on the field at the rightmost boundary, the propagation matrix should relate the field at $z = 0$ to the field at $z = l$.

$$\begin{bmatrix} \tilde{E}_+(0) \\ \tilde{E}_-(0) \end{bmatrix} = \begin{bmatrix} e^{-ikl} & 0 \\ 0 & e^{ikl} \end{bmatrix} \begin{bmatrix} \tilde{E}_+(l) \\ \tilde{E}_-(l) \end{bmatrix} \tag{1.15}$$

The Propagation Matrix P is defined for a layer of depth l as

$$P = \begin{bmatrix} e^{-i\tilde{k}l} & 0 \\ 0 & e^{i\tilde{k}l} \end{bmatrix} \tag{1.16}$$

Note that the wavenumber $\tilde{k}$ has been changed to a complex value in Equation (1.16). This accounts for the fact that the index of refraction $\tilde{n}$ can be complex-valued, as shown previously, and $\tilde{k} = \frac{\tilde{n}\omega}{c}$. The wavenumber up to this point has been referred to as k for clarity, but now, it is important to clarify that it may include an imaginary component, and the math will remain the same. If we substitute $\tilde{k}$ for k, we can see how this might affect our propagation matrix:

$$k = \frac{n\omega}{c} \Longrightarrow \tilde{k} = \frac{(n + i\kappa)\omega}{c} = k + i\kappa' \tag{1.17}$$

Now, wavenumbers can also include an imaginary component κ'. The imaginary component multiplied by the imaginary unit in in the exponents of (1.16) yields real-valued factors that alter the propagating waves. As shown, if $\tilde{n}$ contains an imaginary component, it manifests as an attenuation factor in the Propagation Matrix:

$$P = \begin{bmatrix} e^{(\kappa' - ik)l} & 0 \\ 0 & e^{(ik - \kappa')l} \end{bmatrix} \tag{1.18}$$

By including the imaginary component of $\tilde{k}$, we see how our propagation matrix also takes care of absorption within linear dielectric media.

1.1.4 Boundary Matrix

While the propagation matrix describes the electric field wave's interactions with layer thicknesses, we also need to account for how the electric field behaves at boundaries between layers in our stack. The boundary matrix is built on the same derivations that were used previously in 1.1.1. Now we define a single boundary (Boundary 1-2) with electric field $\tilde{E}_1$ on the left side of the boundary and field $\tilde{E}_2$ on the right side, along with indices of refraction of the two dielectric materials, n_1 and n_2, respective to the field indices.

The boundary conditions (iii) and (iv) inform us that the parallel components of the electric fields and magnetic fields must be continuous across any boundary. Since we are looking at normally incident waves, and the waves are transverse in nature, the electric

and magnetic fields are parallel to the surface of the boundary, and these boundary conditions apply directly in our setup. From electromagnetic boundary condition (iii) and (iv), we find, respectively:

$$\tilde{E}_{1+} + \tilde{E}_{1-} = \tilde{E}_{2+} + \tilde{E}_{2-}$$
$$n_1[\tilde{E}_{1+} - \tilde{E}_{1-}] = n_2[\tilde{E}_{2+} - \tilde{E}_{2-}]$$

Some algebraic rearrangement can lead us from here to expressions for $\tilde{E}_1+$ and $\tilde{E}_1-$. (Adding and subtracting the two equations above yields these relationships.)

$$\tilde{E}_{1+} = \frac{1}{2n_1}[(n_1 + n_2)\tilde{E}_{2+} + (n_1 - n_2)\tilde{E}_{2-}]$$
$$\tilde{E}_{1-} = \frac{1}{2n_1}[(n_1 - n_2)\tilde{E}_{2+} + (n_1 + n_2)\tilde{E}_{2-}]$$

For the purposes of a Transfer Matrix, these are better expressed in factored matrix form:

$$\begin{bmatrix} \tilde{E}_{1+} \\ \tilde{E}_{1-} \end{bmatrix} = \frac{n_1 + n_2}{2n_1} \begin{bmatrix} 1 & \frac{n_1 - n_2}{n_1 + n_2} \\ \frac{n_1 - n_2}{n_1 + n_2} & 1 \end{bmatrix} \begin{bmatrix} \tilde{E}_{2+} \\ \tilde{E}_{2-} \end{bmatrix} \tag{1.19}$$

It is more convenient to define the terms τ and γ to clean up the Boundary Matrix notation.

$$\tau = \frac{2n_1}{n_1 + n_2}$$

$$\gamma = \frac{n_1 - n_2}{n_1 + n_2}$$

Finally, the Boundary Matrix M can be written as

$$M = \frac{1}{\tau} \begin{bmatrix} 1 & \gamma \\ \gamma & 1 \end{bmatrix} \tag{1.20}$$

This matrix, similar to (1.16), relates the fields on the right side of a boundary to find the fields on the left side of that boundary. This is how our matrix will operate. Now we have Propagation Matrix P and Boundary Matrix M relating the amplitude of the fields across the layers and boundaries of a dielectric stack.

1.1.5 Transfer Matrix

Now, the Propagation and Boundary Matrices can be used to generalize the formation of a Transfer Matrix. For a multi-layered dielectric media stack with $N + 1$ boundaries and N layers (see Figure 1.2), we can define Propagation Matrices through each layer P_j for $j = 1, 2, ..., N$ and Boundary Matrices $M_{i,j}$ for $i = 0, 1, 2, ..., N$, and $j = 1, 2, 3, ..., N + 1$.

To relate the fields on either end of the stack, we define the Transfer Matrix T

$$T = M_{0,1}P_1M_{1,2}P_2...P_{N-1}M_{N,N+1}$$

If we remove one matrix from T at a time, starting with $M_{0,1}$, we can get a glimpse of the electric fields within the dielectric stack at either side of any boundary, with each of the matrices modeling light's interaction with a specific feature of the material. All together, the transfer matrix describes the total structure of the material, and models light's interaction with it.

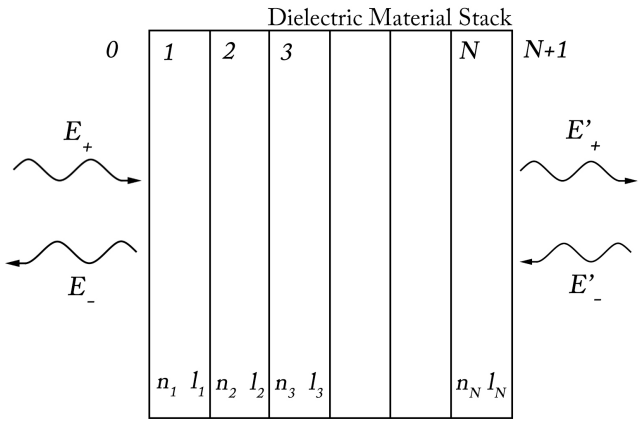

Figure 1.2: A dielectric material stack, with electric field components E_+, E_-, E'_+, and E'_-. The transfer matrix uses refractive indices n_i and layer thicknesses l_i to relate the fields on either side of the stack.

The entire transfer matrix will describe, more specifically, the relation between forward and backward propagating electric field waves on either side of the dielectric stack. Using the notation $E_{+,-}$ to represent the electric field's forward and backward propagating components on the left edge of the dielectric stack, and $E'_{+,-}$ to represent the same components of the electric field on the right edge of the dielectric stack:

$$\begin{bmatrix} E_+ \\ E_- \end{bmatrix} = T \begin{bmatrix} E'_+ \\ E'_- \end{bmatrix} \tag{1.21}$$

A particularly useful application of the Transfer Matrix Method is the calculation of reflectance from a material. We can define the reflection coefficient as the ratio between the reflected and incident electric fields:

$$\Gamma = \frac{E_-}{E_+} \tag{1.22}$$

Focusing on this use in particular, we can choose to set E'_- to zero, modeling light incident only from the left. Without a source on the right side, $E'_- = 0$. By doing this, we may choose an arbitrary value of E'_+, as both E_+ and E_- will be a linear function of E'_+, and the reflection coefficient is defined as the ratio between them.

The reflectance of a material is defined as the ratio of the intensities of the reflected

and incident electric fields. Recalling (1.9), intensity is proportional to the square of the electric field, and the refractive index of the material. Since both the reflected and incident light are propagating through the same medium with the same refractive index (the leftmost layer), the ratio of the intensities $\frac{I_R}{I_I}$ depends only on the ratio of the electric fields, squared.

$$\frac{I_R}{I_I} = \left(\frac{E_-}{E_+}\right)^2 = \Gamma^2 \tag{1.23}$$

It follows that the reflectance Γ^2 of the material for light of frequency ω takes on a value between 0 and 1.

The usefulness of the transfer matrix will be elaborated on in Sections (II) and (III), but it is important to reflect on the physical interpretation of what we have derived. Our transfer matrix can be used to describe the intensity of reflection for light of a given wavelength incident on a multi-layered stack of dielectric materials, each with a complex refractive index that does not vary through a single layer. We have assumed normal incidence of the waves on the stack, and we know that any oblique angle incidence would change the results, since the optical path length through a single dielectric stack is increased with angle of propagation. Oblique incidence would also require knowledge of the polarization of incident light, since parallel and perpendicular polarizations will reflect differently. We have also assumed perfectly smooth surfaces, which lead to perfect reflection and transmission described by Fresnel's Equations.

In practice, the TMM will only act as a model for an ideal material stack. Real manufacturing methods and environmental conditions may produce imperfect boundaries and non-homogeneous dielectric layers. In this way, the Transfer Matrix will provide an approximation for a structure, but its results should be approached with caution. The TMM approach offers scalability, which can also be applied to a continuously varying medium by discretizing the medium into thin slices.

1.2 Acoustic Equivalence

Given the established transfer matrix method of modeling reflections and transmissions for electromagnetic waves, we should be able to perform similar computations for all phenomena that have wave-like behavior. The wave-like nature of light cues us into its usefulness for modeling other waves, like acoustic waves. Sound is the human response to slight changes in pressure in the air around us. These pressure changes propagate as acoustic waves. Like electric field waves, their velocity in a material depends on some intrinsic property of the material. Similar to how the index of refraction could predict the speed of light in a medium, density can predict the speed of acoustic waves in media as well. A derivation of the reflection and transmission of sound at a boundary can convince us that the transfer matrix may have similar utility in the domain of acoustics.

1.2.1 Acoustic Reflection and Transmission

Sound propagates as small changes in pressure in gases, liquids, and solids. One of the biggest differences between propagation of light waves and sound waves is that sound waves must have a medium through which to travel. This medium will always have an intrinsic density and pressure, so we must model the waves that carry sound as small changes in the intrinsic density and pressure.

$$P = P_0 + p \ \textit{(Pressure)} \tag{1.24}$$

$$\rho = \rho_0 + \delta \ \textit{(Density)} \tag{1.25}$$

where $p \ll P_0$ and $\delta \ll \rho_0$. Changes in the density of a medium lead to changes in the pressure of the medium, which create further changes in density, leading to the phenomenon of waves. To derive this connection, we must first derive the acoustic wave equation [5]

If we assume that pressure is some function of density $P = f(\rho)$, then we can say, with a first order Taylor expansion,

$$P_0 + p = f(\rho_0 + \delta) = f(\rho_0) + \delta f'(\rho_0) \tag{1.26}$$

Isolating the second term, we can re-express it as

$$p = \delta\Big(\frac{dP}{d\rho}\Big)_{\rho_0} \tag{1.27}$$

Now we introduce the first continuity condition: that the displacement of particles disturbed by sound waves must be continuous. Succinctly, if the displacement of a particle at position x is denoted $\xi(x)$, then it follows that

$$\xi(x + \Delta x, t) = \xi(x, t) + \frac{\partial \xi}{\partial x}\Delta x \tag{1.28}$$

Given this statement, we can describe changes in the density, as well. Changes in density are also small, so we can express how the density change is related to the change in displacement. Since we are focusing on all of these quantities in a single dimension, we can identify that mass can be described as density times a distance. Conservation of mass with changes in displacement and density gives us:

$$\rho_0 \Delta x = \rho(\frac{\partial \xi}{\partial x}\Delta x + \Delta x) \tag{1.29}$$

$$\rho_0 = (\rho_0 + \delta)\frac{\partial \xi}{\partial x} + \rho_0 + \delta \tag{1.30}$$

Subtracting ρ_0 from both sides and remembering that $\delta \ll \rho_0$ we can arrive at an expression for δ

$$\delta = -\rho_0 \frac{\partial \xi}{\partial x} \tag{1.31}$$

Now we must add the second continuity condition. This condition follows from Newton's First Law, and states that pressure must also be a continuous function, since the forces acting on every particle must be balanced. If a small mass of air $\rho_0 \Delta x$ has some acceleration related to its displacement as $\frac{\partial^2 \xi}{\partial t^2}$, the force in the x direction is given by

$$P(x,t) = \rho_0 \Delta x \frac{\partial^2 \xi}{\partial t^2}|_x \tag{1.32}$$

Given the second continuity condition, we can find that

$$P(x,t) - P(x+\Delta x, t) = -\frac{\partial P}{\partial x}\Delta x = -\frac{\partial p}{\partial x}\Delta x \tag{1.33}$$

with the last equivalence given by the logic that when P changes, P_0 stays constant and p varies. We can now say

$$\rho_0 \frac{\partial^2 \xi}{\partial t^2} = -\frac{\partial p}{\partial x} \tag{1.34}$$

Subbing in from equation (1.27), we find that

$$\rho_0 \frac{\partial^2 \xi}{\partial t^2} = -\Big(\frac{dP}{d\rho}\Big)_{\rho_0} \frac{d\delta}{dx} \tag{1.35}$$

and then, using (1.31), we find

$$\frac{\partial^2 \xi}{\partial t^2} = \Big(\frac{dP}{d\rho}\Big)_{\rho_0} \frac{\partial^2 \xi}{\partial x^2} \tag{1.36}$$

By assuming that $\left(\frac{dP}{d\rho}\right)_0 = c^2$ for c the speed of sound in a material, we have derived a wave equation for sound,

$$\frac{\partial^2 \xi}{\partial x^2} = \frac{1}{c^2}\frac{\partial^2 \xi}{\partial t^2} \tag{1.37}$$

With the wave equation in place, we can now refer back to the continuity conditions for acoustic waves to study how they might behave at boundaries between materials.

$$\xi = \xi' \tag{1.38}$$

$$p = p' \tag{1.39}$$

That is to say changes in displacement, and changes in pressure are continuous functions within the wave, and must therefore be continuous across boundaries as well. We can relate pressure changes to displacement just as we were able to relate electric fields to magnetic fields for the electromagnetic wave equations, as the two are intrinsically connected in a similar way.

To build the wave equation for acoustic waves, we set $\left(\frac{dP}{d\rho}\right)_{\rho_0} = c^2$. Referring back

to equations (1.27) and (1.31), we can make similar substitutions, as they were fundamental to building our wave equation.

$$p = \delta\Big(\frac{dP}{d\rho}\Big)_{\rho_0} = -\rho_0 c^2 \frac{\partial \xi}{\partial x} \tag{1.40}$$

Now we have expressions for both of our continuity conditions in terms of one variable, ξ. Equation (1.40) is the acoustic equivalent to equation (1.2). This allows us to move forward quickly with the same analysis that we used in the electromagnetic case. The incident, reflected, and transmitted waves at a boundary are given by:

$$\begin{aligned}
\tilde{\xi}_I(z,t) &= \tilde{\xi}_{I_0} e^{i(k_I z - \omega t)} & \tilde{p}_I(z,t) &= -ik_I \rho c^2 \tilde{\xi}_{I_0} e^{i(k_I z - \omega t)} \\
\tilde{\xi}_R(z,t) &= \tilde{\xi}_{R_0} e^{i(k_R z - \omega t)} & \tilde{p}_R(z,t) &= -ik_R \rho c^2 \tilde{\xi}_{R_0} e^{i(k_R z - \omega t)} \\
\tilde{\xi}_T(z,t) &= \tilde{\xi}_{T_0} e^{i(k_T z - \omega t)} & \tilde{p}_T(z,t) &= -ik_T \rho c^2 \tilde{\xi}_{T_0} e^{i(k_T z - \omega t)}
\end{aligned}$$

For the pressure waves, replacing k by $\frac{\omega}{c}$ and ρ and c by ρ_i and c_i is useful, as the incident and reflected waves travel in the same medium, but in the opposite direction.

$$\begin{aligned}
\tilde{p}_I(z,t) &= -i\omega \rho_1 c_1 \tilde{\xi}_{I_0} e^{i(k_1 z - \omega t)} \\
\tilde{p}_R(z,t) &= i\omega \rho_1 c_1 \tilde{\xi}_{R_0} e^{i(-k_1 z - \omega t)} \\
\tilde{p}_T(z,t) &= -i\omega \rho_2 c_2 \tilde{\xi}_{T_0} e^{i(k_2 z - \omega t)}
\end{aligned}$$

Applying boundary conditions (1.38) and (1.39), we find the following

$$\tilde{\xi}_{0I} + \tilde{\xi}_{0R} = \tilde{\xi}_{0T} \tag{1.41}$$

$$\rho_1 c_1 (\tilde{\xi}_{0I} - \tilde{\xi}_{0R}) = \rho_2 c_2 \tilde{\xi}_{0T} \tag{1.42}$$

.

By defining the specific impedance of a material Z to be

$$Z = \rho c \tag{1.43}$$

we find, through algebraic rearrangement, the acoustic equivalent to Fresnel's Equations (1.7) and (1.8), in terms of specific impedance.

$$\xi_{0R} = \frac{Z_1 - Z_2}{Z_1 + Z_2} \xi_{0I} \tag{1.44}$$

$$\xi_{0T} = \frac{2Z_1}{Z_1 + Z_2} \xi_{0I} \tag{1.45}$$

The ratio of the intensities defines the reflection and transmission. Intensity

$$I = \frac{1}{2}\rho c \xi^2 \omega^2 \tag{1.46}$$

leads to

$$\frac{I_R}{I_I} = \frac{\xi_{0R}^2}{\xi_{0I}^2} = \Big(\frac{Z_1 - Z_2}{Z_1 + Z_2}\Big)^2 \tag{1.47}$$

$$\frac{I_T}{I_I} = \frac{Z_2}{Z_1}\frac{\xi_{0T}^2}{\xi_{0I}^2} = \frac{Z_2}{Z_1}\Big(\frac{2Z_1}{Z_1 + Z_2}\Big)^2 \tag{1.48}$$

To develop the transfer matrix for acoustic reflections, we can follow the same logic we used to develop the electromagnetic transfer matrix. It is once again useful to split up the displacement wave into forward and backward traveling components, ξ_+ and ξ_-.

$$\tilde{\xi}(z,t) = \tilde{\xi}_+ e^{i(kz-\omega t)} + \tilde{\xi}_- e^{i(-kz-\omega t)} \tag{1.49}$$

We will look for an acoustic transfer matrix that models the system

$$\begin{bmatrix} \xi_+ \\ \xi_- \end{bmatrix} = T_A \begin{bmatrix} \xi'_+ \\ 0 \end{bmatrix}$$

where $\xi'_{+,-}$ denotes the displacement to the immediate right of the boundary, and $\xi_{+,-}$ denotes the displacement immediately to the left. Just as in the electromagnetic case, we set $E'_- = 0$ so that we are only calculating reflections. We can then populate our transfer matrix with propagation and boundary matrices, just as we did in the electromagnetic case.

1.2.2 Propagation Matrix

We can describe the spatial propagation of forward an backward propagating acoustic waves through a layer of thickness l with the following formula:

$$\tilde{\xi}_+(z) = \tilde{\xi}_+(0)e^{ikz}$$
$$\tilde{\xi}_-(z) = \tilde{\xi}_-(l)e^{ik(l-z)}$$

This leads to the same propagation matrix that we found in equation (1.16).

$$\begin{bmatrix} \tilde{\xi}_+(0) \\ \tilde{\xi}_-(0) \end{bmatrix} = \begin{bmatrix} e^{-ikl} & 0 \\ 0 & e^{ikl} \end{bmatrix} \begin{bmatrix} \tilde{\xi}_+(l) \\ \tilde{\xi}_-(l) \end{bmatrix} \tag{1.50}$$

$$P = \begin{bmatrix} e^{-ikl} & 0 \\ 0 & e^{ikl} \end{bmatrix}$$

This Propagation Matrix describes the propagation of the acoustic waves through a medium of thickness l, in exactly the same way as the electric field propagation matrix did. This is unsurprising, considering that the wave equations do not differ except for the physical quantity that is oscillating in the wave.

1.2.3 Boundary Matrix

Following an analogous approach to section 1.2.2, we begin with our continuity conditions (1.38) and (1.39), and apply our new formulation of the displacement (1.49):

$$\tilde{\xi}_+ + \tilde{\xi}_- = \tilde{\xi}'_+ + \tilde{\xi}'_-$$
$$Z_1(\tilde{\xi}_+ - \tilde{\xi}_-) = Z_2(\tilde{\xi}'_+ - \tilde{\xi}'_-)$$

Algebraic rearrangement leads to the following equation, in matrix form:

$$\begin{bmatrix} \tilde{\xi}_+ \\ \tilde{\xi}_- \end{bmatrix} = \frac{Z_1 + Z_2}{2Z_1} \begin{bmatrix} 1 & \frac{Z_1 - Z_2}{Z_1 + Z_2} \\ \frac{Z_1 - Z_2}{Z_1 + Z_2} & 1 \end{bmatrix} \begin{bmatrix} \tilde{\xi}'_+ \\ \tilde{\xi}'_- \end{bmatrix} \tag{1.51}$$

This is also of the same form as the electromagnetic equivalent, with the specific impedance Z substituted for index of refraction n. We might notice that the specific impedance and refractive index describe a similar property: how fast waves move through the medium.

We can also simplify the equation above by reintroducing coefficients τ and γ.

$$\tau = \frac{2Z_1}{Z_1 + Z_2} \tag{1.52}$$
$$\gamma = \frac{Z_1 - Z_2}{Z_1 + Z_2} \tag{1.53}$$

With these definitions, we now can build the exact same boundary matrix as in the electromagnetic case, with the only difference being the formulation of τ and γ.

$$M = \frac{1}{\tau} \begin{bmatrix} 1 & \gamma \\ \gamma & 1 \end{bmatrix} \tag{1.54}$$

This formulation allows for us to easily convert electric field wave propagation calculations into acoustic ones, as we construct our entire transfer matrix.

1.2.4 Transfer Matrix

To arrive at our final acoustic wave transfer matrix, we set up our structure the same way as in the electromagnetic case, with a stack of materials N+1 layers thick, with N borders. We are looking for the displacement on the left-most edge of the stack as a function of the displacement on the right-most edge, so we will left multiply the displacement on the right until we reach the left-most boundary.

$$T_A = M_1 P_1 M_2 P_2 ... P_{N-1} M_N$$

The transfer matrix builds the relationship

$$\begin{bmatrix} \tilde{\xi}_+ \\ \tilde{\xi}_- \end{bmatrix} = T_A \begin{bmatrix} \tilde{\xi}'_+ \\ \tilde{\xi}'_- \end{bmatrix} \tag{1.55}$$

The transfer matrix accounts for all internal reflections and transmissions, leading to an easy calculation which can describe the complex phenomenon of reflection and transition within layered media. If we set the right incident wave $\tilde{\xi}'_-$ to 0, we can simulate the desired setup for our experiments, with sound incident on only the left edge of the stack, propagating and reflecting through it. Similar to the case of electromagnetic reflection, our reflection coefficient is given by

$$\Gamma = \frac{\tilde{\xi}_-}{\tilde{\xi}_+} \tag{1.56}$$

The ratio does not depend on any chosen value of $\tilde{\xi}'_+$, so its value can be set arbitrarily. The reflectance of the incident wave is once again given by the ratio of the intensity of the reflected wave to the incident wave.

$$\frac{I_R}{I_I} = \Gamma^2 = \left(\frac{\tilde{\xi}_-}{\tilde{\xi}_+}\right)^2 \tag{1.57}$$

It is useful to reflect on the Acoustic Wave Transfer Matrix just as we did for the Electromagnetic Wave Transfer Matrix, as our model describes only an ideal material stack.

The Acoustic Wave TMM describes the reflection of normally incident sound waves of a single frequency from a multi-layered material, where each layer of the material consists of a homogenous density ρ and speed of sound c. The normal incidence of the waves is important, as any oblique angle would produce a different acoustic path length for the wave propagation. While we would not have to worry about polarization of the wave like we did with light, since acoustic waves propagate longitudinally, we would have to take into account different complications that arise from acoustic waves. Specifically, for material solids, whose individual molecules are held together by bonding, acoustic waves can produce vibrations in the material. These vibrations in spatially finite structures could be coupled to otherwise orthogonal modes that can propagate as surface waves, and can strongly interfere with TMM calculated reflections.[6] This means that normal propagation must be imposed in experiments in order for models to agree with experimental results.

Furthermore, we have again assumed a smooth surface for our reflections and transmissions. Although this is a close approximation, it is not sufficient in every case. As such, the transfer matrix should be used with knowledge of its usefulness and limitations.

Chapter 2

Methods of Structural Coloration Enhancement in a Colorimetric Sensing Material

Colorimetric sensing technology offers the means for rapid, inexpensive, portable, always-on, wearable, and reliable detection of chemicals in an environment. In visual colorimetry, sensor materials produce an observable color-change at their surface in response to the presence of environmental stimuli. Traditional colorimetric sensors have employed the use of a chemically-reactive and relatively thick (order of microns) sensor material to produce chemical coloration. As a reaction takes place, the chemical change induces a color-change at the sensor surface, alerting an observer to the presence of the environmental stimulus. Structural coloration is assessed for its potential or promise in enhancing this color change. Here, we present methods for utilizing structural coloration for the improvement of colorimetric sensing materials, which may lead these materials to faster response times, lower detection limits, and enhanced color-change.

Colorimetric sensors offer a simple yet effective approach to the detection of chemicals in an environment. With the use of a chemically-reactive material, chemical agents are allowed to passively diffuse into the material, inducing a chemical reaction with sensor materials. This change alters the material's optical properties, inducing a change in its reflection spectrum and observable color. Such technology has applications in the detection of dangerous chemical toxins given its low power consumption, portability, agent selectivity, and the intrinsic reactivity of the toxins.[7, 8] Both indicator papers and reagent arrays can be created to test for a number of chemical agents at once, widening the application of the technology further. [9, 7, 10] As the need for easily deployable, low power colorimetric sensors grows, the design of the sensors and the manipulation of color in chemical detection becomes more important.

Changes in the reactive surface's absorption spectrum can be measured with spectroscopy, providing quantitative data about the presence of chemical agents.[11] A spec-

trometer can measure slight changes in the shape of a spectrum, while a photodiode can measure the fine changes at individual wavelengths. Both types of data can be useful in the detection of specific stimuli. However, the spectroscopic measurement approach to colorimetry can require bulky expensive equipment and an external power supply. The human eye has its own spectral analysis capabilities, evident in our perception of color. Colorimetric sensors that produce perceptible changes in observable surface color can be just as useful to the detection of chemicals as those that produce spectroscopically measureable changes, if not more so. A challenge in the case of visual colorimetry is producing perceptible color changes through the reaction of a chemical agent with a chemochromic reagent surface.

Existing techniques for colorimetric sensing have used chemical coloration to produce visually and spectroscopically measureable changes at the sensing material surface after the adsorption of a chemical agent from the environment. [12, 13, 9, 7, 11, 14, 15] Chemical coloration is central to colorimetry. The passive diffusion of chemical agents into chemochromic reagent surfaces (often a hydrogel-based compound) makes the delivery and detection of agents easy. [13, 12, 16] These surfaces can undergo a reaction with the chemical agents, changing their optical properties, altering their absorption and reflection spectra, and in turn, their color. If the reagent is chosen correctly, an observable color-change can be elicited through this diffusion and adsorption.

However, the utility of chemical coloration is limited—ranges in sensitivity make many sensors unsuitable in environments other than those with high concentrations of chemical agents. Additionally, the utility of chemical coloration in colorimetric sensing is limited by the color-change response time, as diffusion of the agent into the sensing layer can take anywhere from seconds to many hours. [7, 11, 13]

Structural coloration has the potential to supplement chemical coloration by enhancing the at-surface color-change of reactive materials, making colorimetric sensing technology more suitable for qualitative assessments by the unaided human eye, as well as providing more spectral contrast for spectroscopic measurements. Structural coloration takes advantage of interference, diffraction, and scattering to selectively interfere specific wavelengths of light, which can effectively reflect light of a desirable color when tuned in the visible range. Structural coloration is a phenomenon that is common in nature—thin film and periodic structure interference is the cause of color in many insects and birds, as well as in inorganic structures (Figure 2.1. [17]

Structure has already been hypothesized to improve the ability of colorimetric chemical sensors to measure spectral changes under different environmental conditions. [18, 16] Additionally, the use of photonic crystals has been shown to increase visible color-changes in response to environmental stimuli through the introduction of a tuneable structure. [19] A Fabry-Perot optical cavity consisting of an optically transparent dielectric layer between a metal substrate and absorber layer has also been shown to be

capable of producing tuneable structural coloration, similar to photonic crystals, but simpler and more scalable.[20] It may also offer promise in enhancing visible colorimetric sensing. In this study, we aim to show through computational simulation that a combination of structural and chemical coloration can produce a desired amplification of color-change in a chemical-sensing material structure.

Our approach to this challenge incorporates the use of an absorber-dielectric-metal optical resonator structure, as described by *Oller et al., 2017*, to maximize the possible color-change of the colorimetric sensing material during reaction with a chemical agent. We chose to focus our attention on the role that structure can play in amplifying chemical induced color-change. Therefore, we chose a single chemochromic reagent material to serve as the representative model for traditional chemical coloration-based colorimetric sensing systems. We chose this material, the absorbing layer of the resonant structure, to be a physical entrapment of 4-(2-pyridylazo)resorcinol (PAR) in sol-gel thin films through a base-catalyzed process, a process which had been previously studied. [21, 14] This layer reacts with Cu(II) ions to produce a noticable change in its absorption spectrum, the chemical-coloration basis for our tests.

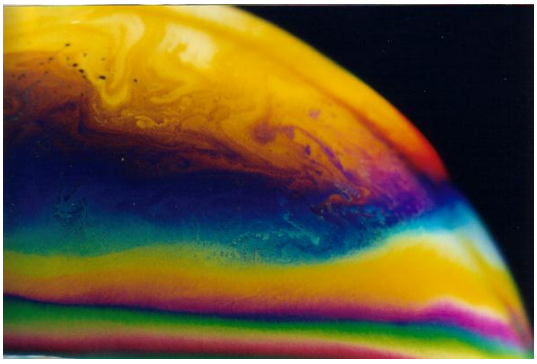

Figure 2.1: An example of structural coloration in nature. Thin film interference produces vibrant colors on the surface of a soap bubble, as colors change with film thickness. Fabry-Perot interference, a similar phenomenon, is hypothesized to augment chemical color changes in colorimetric sensing material. (©User: Threetwoone / Wikipedia Commons / CC-BY-2.5)

We chose to use silicon dioxide SiO_2 as our optically transparent dielectric phaser layer. This layer acts as the cavity space for resonance in the Fabry-Perot optical cavity. The phaser layer adjusts the phase of the light waves propagating through the structure, setting up interference at specific wavelengths. SiO_2 is chemically inert in the presence of Cu(II) ions, ensuring that its effect on coloration is purely structural, and that it does not interfere with the chemical coloration provided by the absorber layer. The thickness of the transparent dielectric layer serves to interfere light of specific wavelengths. For the substrate, which completes the Fabry-Perot optical cavity structure, we chose to experiment with two different materials: silicon (Si) and Aluminum (Al). These substrates are both reflective and highly absorbent, ensuring that all light at the surface of the PAR layer is reflected or absorbed, and cannot transmitted to or from

the back side of the sample.

Color change amplifications may also lead to opportunities for faster and more sensitive response to stimuli. With amplification from structural coloration, a colorimetric sensing material can produce equal response given less stimulation, as the tuneable Fabry-Perot optical cavity could be used to adjust amplitude of the color-change. With amplification from such a cavity, similar color response can be produced with a thinner absorber layer, lower stimulus concentrations, shorter exposure times, or any combination of the three.

In this study, we aimed to show the possibility of color-change amplification through simulation. The Transfer Matrix Method (TMM) offers a simple approach to the simulation and optimization of different potential colorimetric sensing structures. As was shown in Chapter 1, the transfer matrix is useful in the determination of reflectance intensity of monochromatic light off a multi-layered dielectric stack. The TMM can perform calculations of reflection for a large number of layers quickly. Given a colorimetric sensing structural design, we were able to use the TMM to simulate its reflectance intensity at discrete wavelength intervals, producing the reflection spectrum of that structure. From reflection spectra, we used color matching functions published by the International Commission on Illumination (CIE) to map the spectral response to quantified human color vision. Through the use of special color spaces, we were not only able to digitally produce the expected color of various structures (as seen with normal human vision), but also to quantify the perceptual difference in surface color before and after the PAR complexation reaction with Cu(II) ions.[22, 23] This quantification of perceptual color difference allowed us to explore the effectiveness of different structures in amplifying color change tailored for direct human vision.

Structural coloration was shown to be a potentially powerful tool in augmenting chemical coloration, and color-change in colorimetric sensor systems. While we were confined to make approximations in our approach to simulations that limited the extent to which we could truly optimize the structure, the use of the PAR absorber as a representative model for a colorimetric chemically-reactive material shows the merits of the use of the TMM and color simulations in optimizing a structure.

2.1 Methods

2.1.1 Material Design

To test our hypothesis, that structural coloration from a Fabry Perot optical cavity could produce an amplified color-change response from a colorimetric material, we chose to apply the idea to an existing colorimetric sensing technology. With a chemical sensing layer that had been previously been shown to have colorimetric sensing capabilities,

we could explore the utility of a structurally enhanced colorimetric sensing material without altering the chemical coloration of the material. Our choice of a physical entrapment of PAR in sol-gel was chosen as a representative model for a colorimetric system based on chemical coloration on which we could test the effects of structure. [14]

The PAR would serve as the absorber layer in our absorber-phaser-substrate Fabry-Perot optical cavity. However, we would also need a control structure against which to test the effects of structural coloration. While it's impossible to eliminate the effects of structural coloration entirely from any material, the elimination of the cavity phaser from the Fabry-Perot optical cavity removes resonance, making resonant interference impossible. As such, a control structure was chosen to consist of a PAR layer directly on top of a substrate.

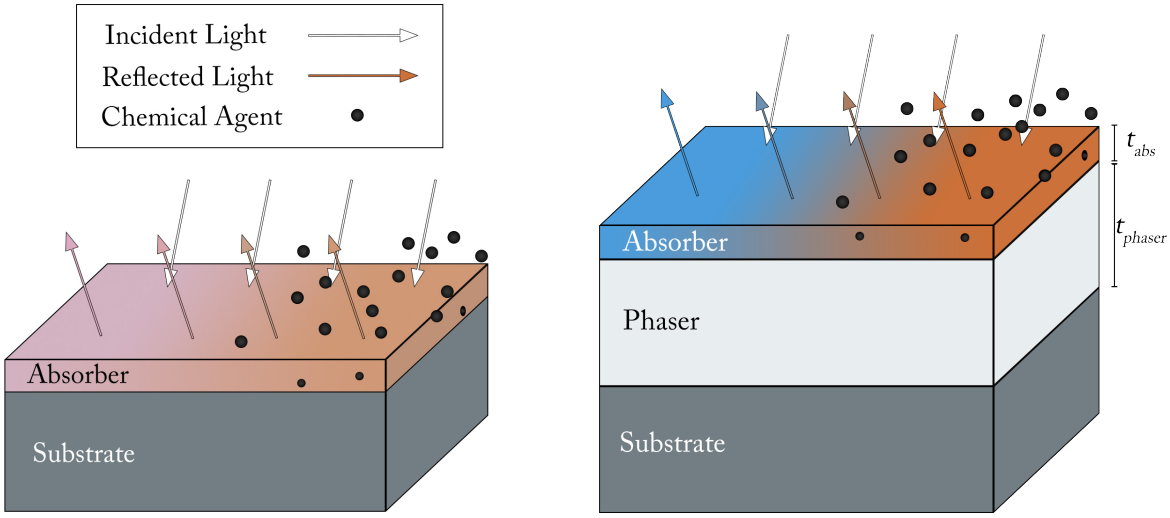

(a) Control Structure (b) Colorimetric Resonator Structure

Figure 2.2: (a) A control structure consists of a metallic substrate beneath a chemically-responsive absorber layer which, in the presence of a chemical agent, undergoes a reaction, shifting its complex refractive index and with it, its reflected color. (b) In the proposed structure, a dielectric resonating layer, referred to as a phaser layer, of thickness t_{phaser} is inserted between the absorber (of thickness t_{abs}) and the metallic substrate. The effect of the phaser is to produce structural coloration through phase interference, which can amplify the changes in the reflection spectrum caused by the absorber layer, creating a more noticeable color-change at surface.

PAR can serve as an optical sensor for the presence of Cu(II) ions. In a study by *Jerónimo et al., 2004*, the PAR was immersed in a low concentration Cu(II) solution (4 $mg\ L^{-1}$), and a PAR-Cu(II) complexation reaction was allowed to occur.[14] Its absorption spectrum was recorded in the visible wavelengths before and after its immersion. The formation of a PAR-Cu(II) complex within the sol-gel entrapment layer

was shown to produce a change in the absorption spectrum of the film. The complex formation led to a decrease in absorption in shorter wavelengths, a new absorption peak around 550nm, and little change in absorption in wavelengths above 600nm. However, the absorption of the complex remained relatively low (below 5%) at all wavelengths, making it optically transparent. For a visually perceived pronounced color change, a thick layer is needed in the absence of an amplification or enhancing mechanism

The reaction of the copper ions with the PAR produces a change that is characteristic of any colorimetric sensing material. With design, any change in absorption spectrum can be exploited so as to produce visual and spectroscopic changes in the presence of the chemical agent. This makes PAR a good model for a colorimetric sensing material, and convenient for us to use in our tests. Its properties are not assumed to lend themselves to structural color-change amplification any better than other colorimetric sensing materials.

Use of the TMM requires the thickness and complex refractive index of each dielectric layer. The real part of the refractive index of our absorber layer, the sol-gel PAR film, was estimated from estimates of the refractive index of electronic-grade silicon dioxide, since sol-gel, after curing, has properties similar to that of a thin film of glass. [24, 14, 25] The imaginary part of the refractive index of the sol-gel PAR film was estimated from its absorption spectrum, before and after the complexation of Cu(II) ions with the PAR immobilized in the sol-gel material. [14] While we were unable to determine the precise refractive index of the material because of the great variance associated with the preparation process and conditions, these estimates provide us with a model for a colorimetric, chemically reactive layer, with which we can probe the merits of structural color amplification with the addition of a phaser layer, creating resonating structure (Fig. 2.2b). With this goal in mind, the exact spectral effects of chemical coloration of material are secondary to the change that occurs in chemical coloration upon reaction. In this light, the materials that we test here should be considered representative models for colorimetric sensing materials, but the results, however, provide a direct assessment of potential and a quantified comparison of a given sensing material with and without the aid of resonant color-change amplification.

To produce structural coloration, which will amplify the chemical color changes from the PAR absorber layer, we chose to experiment with the simplest Fabry-Perot resonating cavity option. Compared to other available options, it is the simplest and most scalable, and can be readily incorporated as a coating layer of a large variety of materials. The planar structure treatment remains valid so long as the lateral dimensions of the material are many times of the wavelengths of interest. This optically transparent, dielectric phaser layer would be tuneable by the thickness of the layer, as select wavelength ranges can be either constructively or destructively interfered. We chose to use silicon dioxide (SiO_2) as the dielectric phaser because of its chemical inertness, low refractive index, and availability. [25] It does not absorb in visible wavelengths due to

its large optical bandgap (9eV), instead serving as the transparent optical cavity of the Fabry-Perot structure.

The Fabry-Perot structure is completed with the addition of a substrate layer. The substrate layers silicon and Aluminum were selected on the bases of high refractive index, availability, and cost.[26, 10] We chose to test two different substrate layers to test the effect of substrate reflectivity on the surface color change. Aluminum is highly reflective and bright white, while silicon is less reflective and dark gray, leading us to expect a brighter color change from the Aluminum substrate material.

The color change due to the chemical reaction in the absorber layer is a caused by a change in the reflection spectrum of the material. In the Fabry Perot structure, the PAR absorber layer and substrate layer act as reflecting interfaces, creating a resonating cavity which can serve to interfere incident light. We can utilize this structure to interfere certain wavelengths, shaping the spectrum of light passing through the absorber layer. If the spectrum of the resonating light is adjusted in a certain way by Fabry-Perot interference, the absorption spectrum change could produce greater contrast in the overall reflection spectrum of the material. For example, if blue wavelengths experience a large change in absorption after the reaction takes place, then destructively interfering red wavelengths and/or constructively interfering blue wavelengths in the phaser layer could serve to make the visual change in "blue-ness" of the material more pronounced. This is the case we hypothesized for the PAR absorbing layer, where the absorption spectrum changes most strongly in the blue region of the spectrum during the reaction with Cu(II) ions.

While we can hypothesize about the effect of interfering certain wavelengths on the reflection spectrum of our material, the actual perception of color is complicated by the human eye's response to different wavelengths (Fig. 2.3), and the resulting change in perceived color. Non-trivial solutions for Fabry-Perot resonant amplification may exist, and would be almost impossible to consider analytically. To account for this, we chose to develop computational methods for the determination of the color change of a given material in the Fabry-Perot configuration. Such methods allow us to quantitatively assess all potential structural designs in our search for color-change amplification. The findings substantatively deviate from the intuitive design guids based on the spectroscopically decompositional F-P cavity analysis, highlighting the spectroscopically convoluted nature of human vision. They also provide definitive support to the notion of color-change amplification by structural coloration and the utility of a different measure of color-change: color distance.

2.1.2 Computational Methods

In Chapter 1, the use of the Transfer Matrix Method was focused on calculating the reflectance of a monochromatic beam off the surface of a multi-layered dielectric ma-

terial. To be useful in calculating a spectral response, this calculation needed to be repeated for many wavelengths covering the optical regime.

Using Matlab, reflectance was calculated for 1001 evenly spaced wavelengths from 390-780nm, an interval width of $\Delta\lambda = 0.389$ nm. This width was chosen so as to provide high resolution reflection spectrum data. In this way, we approximated white, incident light to be made up of equal contributions from each of these wavelengths. In order to ensure that incident light would either be absorbed or reflected (not transmitted), the thickness of the substrate was defined as 1cm in simulations, far greater than its optical thickness. (Fig. 2.3)

Refractive index $\tilde{n}$ can be complex valued, as we recall from Section 1.1.3, but it also takes on different values for different wavelengths. This somewhat complicated calculations, as we needed to know both the real and imaginary components of the refractive index for every wavelength to be tested. Complex refractive indices were drawn from previous studies on materials which covered the optical wavelengths. The data on refractive indices across the optical wavelength range was interpolated onto query points and tested using the TMM. For each wavelength reflectance test carried out by the TMM Matlab code, the corresponding refractive indices for that wavelength were used to model the material.

In order to quantify color change, we first needed a way to quantify color. The Transfer Matrix Method produces a reflection spectrum, given an assumed perfect illuminant with equal spectral intensity across all wavelengths. This uniform spectral intensity assumption can be removed and replaced by solar spectrum to better correspond to the in-field operation of colorimetric sensing. The reflection spectrum gives the percentage of incident light reflected at each wavelength (the remaining light is absorbed by the material). However, human vision does not sense all optical wavelengths uniformly. Human vision roughly covers a range of wavelengths from 390-780nm, through the use of three distinct cone cell photoreceptors within the retina. Each photoreceptor is sensitive to a different range of wavelengths, generally regarded to cover the red, green, and blue parts of the spectrum.[27] However, the intensity response of each cell is wavelength specific.

With this visual system in mind, we sought to determine the human eye's response to an arbitrary reflection spectrum. A number of color spaces have been defined by the International Commission on Illumination / Commission Internationale de l'Eclairage (CIE) to serve different purposes in the quantification of color. The CIE 1931 color matching functions specify how the cones in our eyes translate different wavelengths into color. [22]. (Fig. 2.3) In this way the Transfer Matrix Method of simulating spectral reflectance could be extended to simulate human perception of visible color. The CIE1931 CIEXYZ space makes available a standard translation from a reflection spectrum to visual color. This color space utilizes three "color-matching functions", which

imitate the spectral sensitivity of each type of cone cell photoreceptor in the human retina. These color-matching functions are defined by the CIE, and denoted $\bar{x}(\lambda)$, $\bar{y}(\lambda)$, and $\bar{z}(\lambda)$.[22] The method for determining the the three coordinates of the color space, $X, Y,$ and Z, is defined for our purposes as follows:

$$X = k \sum_{\lambda} R(\lambda)\bar{x}(\lambda)\Delta\lambda \tag{2.1}$$

$$Y = k \sum_{\lambda} R(\lambda)\bar{y}(\lambda)\Delta\lambda \tag{2.2}$$

$$Z = k \sum_{\lambda} R(\lambda)\bar{z}(\lambda)\Delta\lambda \tag{2.3}$$

where $R(\lambda)$ is the reflection spectrum, and $k = 1/\sum_{\lambda} \bar{y}(\lambda)\Delta\lambda$, a normalizing constant to ensure that X, Y, and Z are all valued between 0 and 1.

The non-linear transformation of a reflection spectrum into the CIEXYZ color space gives us a way to quantify the color that a person with normal vision would see when looking at an arbitrary layered material. However, for the purposes of visual colorimetry, one would be more interested in the color-change that a person would see when looking at a material undergoing a reaction with a chemical agent. Euclidean distance in the CIE (human perception) color space offers a promising method for computing the difference between two colors, since the X, Y, and Z coordinates make up a Euclidean space, but the CIEXYZ space was not developed with perceptual uniformity in mind. Perceptual uniformity is the property of a color space that equal Euclidean distances in the space correspond with equal differences in perceived color.[28] Although two distances in the CIEXYZ space may be equal, they represent different shifts in perception.

CIELab is an alternative color space, developed with perceptual uniformity in mind. The color space meets our requirement, that equal distances between points correspond with equal differences in color perception, and has been shown to be useful for color reproduction on metallic substrates.[29, 30] In this color space, the three coordinates $L^*, a^*,$ and b^* represent lightness, the red-green axis, and the yellow-blue axis respectively. Color differences d are defined between two points (L_1^*, a_1^*, b_1^*) and (L_2^*, a_2^*, b_2^*) as

$$d = \sqrt{(L_1^* - L_2^*)^2 + (a_1^* - a_2^*)^2 + (b_1^* - b_2^*)^2} \tag{2.4}$$

To use this color space, we transformed color from the CIEXYZ color space to the CIELab color space using the transformations described by the CIE. [23] The CIELab space is widely-used, so software such as Adobe Photoshop can be used to reproduce the color visually (as was done and labeled in some figures of this thesis).

The quantification of color in this way allows us to holistically describe the change in the reflection spectrum that occurs in the presence of the chemical agent, based on

the human eye's response to that change. A measurement of color difference using CIELab is equivalent to a measurement of the perceptual color change that a person with normal vision would observe at a material's surface. Furthermore, calculation of color using the CIELab coordinate system makes it easy to simulate the physical color that will be observable on the surface. By applying these two color spaces in our simulations, we can effectively quantify and visualize the color of the colorimetric sensing material before the reaction with Cu(II), after the reaction, and the perceived difference between the two.

2.1.3 Methods of Optimization

With the tools that have been developed, we can run simulations to optimize the performance of an absorber-phaser-substrate colorimetric sensing structural design. We can measure the performance of a candidate structure in a number of ways. The structure's performance could be assessed by the response time of chemicals to the absorbing layer (yielding the fastest color-change response). The performance could also be measured by the chemical agent concentration that yields a perceivable color change. In this work, however, we are looking to see what kind of color-change amplification is possible with the addition of a phaser layer, so we will focus our simulations solely on the performance of the material in this regard.

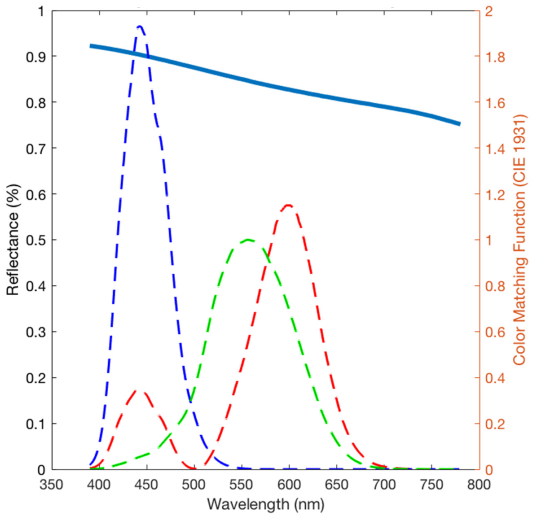

Figure 2.3: **Reflectance and Human Vision** An example reflectance spectrum, $R(\lambda)$, calculated by the TMM for a 100nm layer of SiO_2 on top of an Al substrate. Also plotted are the three color matching functions ($\bar{x}(\lambda)$, $\bar{y}(\lambda)$, and $\bar{z}(\lambda)$) defined by the CIE in 1931, which correspond with each cone's intensity normalized wavelength sensitivity, and transform the spectrum into the CIEXYZ color space.

In its nature, a color-changing sensor is meant to undergo a color change, so it is this metric which we will attempt to optimize, using the quantitative techniques described in the previous section. The metric d (color difference) represents the Euclidean distance between two colors in the CIELab color space.

We have already determined the materials which we will use in the experiments, so all that is left to optimize in this case is the physical dimensions of the material. We

have seen that by varying thickness of the phaser layer, different colors can be produced at the surface, a result of structural coloration. We also have outlined the goal of "shaping" the spectrum of available light through use of the phaser layer, such that the absorber layer absorption changes yield higher-contrast spectral reflectance changes from the structure as a whole. Thus, we should aim to vary the thickness of the resonant phaser layer t_{phaser} such that we find thicknesses which induce structural color-change amplification.

However, it is possible that the thickness of the absorber layer (t_{abs}) will play a role in the performance of a sensing structure. The thickness of the absorber has two possible effects on the performance of the device: the absorber in its nature absorbs light, so the a thicker absorber layer means greater absorption, but it also offers the opportunity for interference in a similar way that the phaser layer does. Sol-gel films on top of SiO_2 produce thin film interference, and for this reason, have been the subject of study in anti-reflective coatings.[31] If this is the case for our PAR layer, its thickness will shape the spectrum of available light for absorption, just as the resonating layer does. We may even consider the likely case that the certain thicknesses of the absorber layer, without the addition of a resonating phaser layer, can produce structural color and possibly a larger color-change.

The manufacture of samples to test a variety of absorber and resonating phaser thicknesses (t_{abs} and t_{phaser}) would be expensive and time-consuming, but with the simulation tools developed, the potential of a multitude of structures can be assessed at once. For tests of colorimetric sensor systems, we varied the absorber layer thickness t_{abs} from 0-500 nm and the phaser layer thickness t_{phaser} from 0-400 nm, both at 5 nm intervals. All combinations of absorber and resonating phaser thicknesses were simulated, giving us an idea of how the color change responds to the addition of a phaser layer for various absorber thicknesses. In addition, two different substrates were used, Si and Al, to see how color-change amplification would be affected by reflectivity of the substrate.

To study the amplification of a color-change by use of a phaser layer, it also proves necessary to define a metric for that amplification. The reference for amplification was chosen to be the Euclidean color difference of the reaction without the addition of a resonating phaser layer (i.e. $t_{phaser} = 0$), called $d^*_{t_{abs}}$. This reference could also be regarded as the "control" that represents the conventional colorimetric sensing approach. If a structure with the same t_{abs}, and some non-zero t_{phaser} has a Euclidean color difference of the reaction $d_{t_{abs}}(t_{phaser})$, then the amplification, $A_{t_{abs}}(t_{phaser})$ is defined to be

$$A_{t_{abs}}(t_{phaser}) = 10 * \log\left(\frac{d_{t_{abs}}(t_{phaser})}{d^*_{t_{abs}}}\right) \tag{2.5}$$

This metric is designed to help study the usefulness of a resonating layer in amplifying color-change, in the case of a particular thickness of the absorber layer, t_{abs}.

In engineering practice, the optimization of a sensor system is a balance between the material selection and physical dimensions. For certain materials, only certain color changes are possible, and so the thicknesses should be arranged in a way that amplifies those changes. Similarly, if thickness is a design and manufacturing constraint, different materials may need to be substituted to amplify color changes in the way we desire. The physical parameters inform the materials, and vice versa. For the purposes of assessing the potential of structural amplification of color-change and the usefulness of the quantification of color-change, however, are constrain the materials to those that we have described, and allow the thicknesses to vary freely, seeing what kind of color-change amplification is possible for an arbitrary but representative colorimetric sensing system.

2.2 Results

2.2.1 TMM and Reflection Spectra Validation

The use of the Transfer Matrix Method to calculate color for colorimetric sensing material structures relies on their ability to calculate reflection spectra. This is the fundamental purpose for the transfer matrix in these experiments, so the validation of the Transfer Matrix Method and its implementation in computational code in calculating reflection spectra is important. To do this, we experimented with two of the materials which we used in the simulation of colorimetric sensing structures: silicon dioxide (SiO_2) and Silicon. The reflectance spectra of two different test samples was and then compared to the reflection spectra calculated using the TMM. The two test samples were 100nm thermally grown SiO_2 on a Silicon wafer, and 300nm thermally grown SiO_2 on a Silicon wafer. The tests were conducted using a reflection spectrometer at 8° incidence angle, so the incident angle in transfer matrix calculations was also set to 8°.

The reflectance spectra measured for these two test samples correspond well with the reflectance spectra calculated using the TMM, with only small differences across optical wavelengths (Fig. 2.4), which is expected given the perfect surface and interface assumed in calculation, and the however small but inevitable deviation in material constants between the actual materials and the computational ones. Although other factors, like the use of exact optical properties corresponding with the actual materials, could affect the use of the transfer matrix, the primary purpose of this study is to explore the possibility of color amplification using phaser structures, a characteristic that can still be studied with imperfect modeling of each material's complex refractive indices and dimensions.

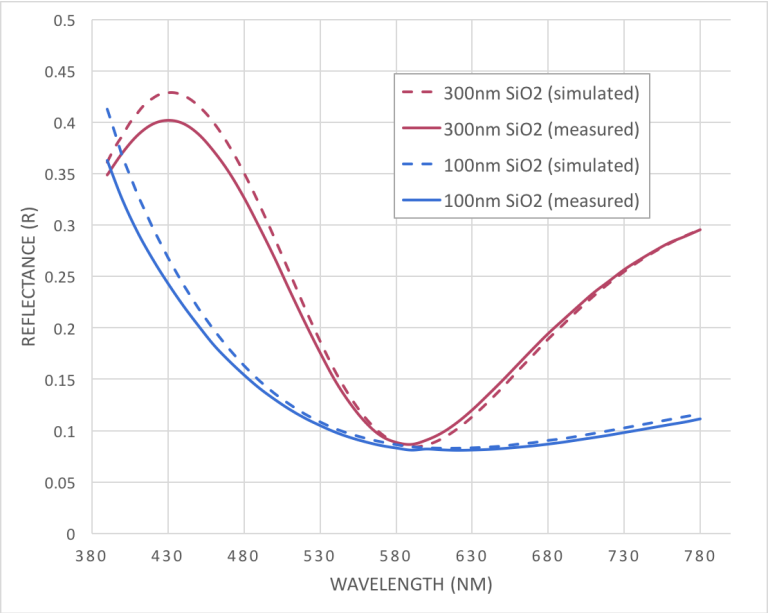

Figure 2.4: Reflection spectra for the two test samples (SiO_2 layer on a Si substrate) used to validate the TMM reflection spectrum calculations. Solid lines indicate measured spectra, and dotted lines indicate spectra simulated using the TMM.

2.2.2 Structurally Altered Color-Change

Turning to the study of the absorber-phaser-substrate colorimetric sensing materials, the effect of structural color in a reaction can be observed with the use of a chromaticity diagram for a single absorber thickness, before and after the PAR reaction with Cu(II) ions (Fig. 2.5). Chromaticity diagrams are derived from the x and y coordinates CIExyY color space, easily transformed from the CIEXYZ space:

$$x = \frac{X}{X+Y+Z} \tag{2.6}$$

$$y = \frac{Y}{X+Y+Z} \tag{2.7}$$

The chromaticity diagram allows us to see changes in the chromaticity of the colors produced in simulations, a quality of color independent of its lightness. These diagrams are useful in studying structural color changes that are induced by changing t_{phaser}.

The chromaticity diagrams show that the structure of the material, namely the thickness of the phaser layer, plays a role in both the color produced and the color change during the reaction. The curves on the two chromaticity diagrams, called color gamuts, have different shapes because of the reaction of PAR with the Cu(II) ions, but the actual individual gamuts are determined by the effect that a phaser layer has on chromaticity. Evidently, structure can alter color-change in colorimetric materials.

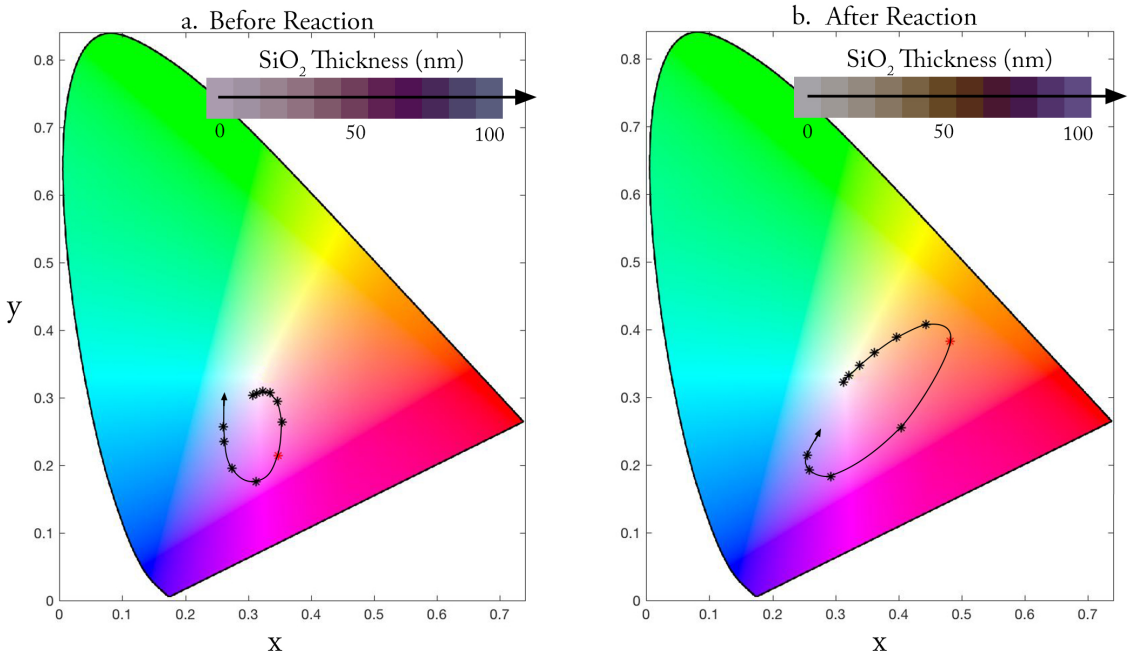

(a) Before Reaction (b) After Reaction

Figure 2.5: Chromaticity changes for a PAR-SiO_2-Si colorimetric sensing material structure, with $t_{abs} = 25$nm. The points $*$ on each diagram indicate the chromaticity with a particular t_{phaser} As the phaser (SiO_2) thickness increases (indicated by $\rightarrow$), the color change between the diagrams changes, because of the effects of structural color. The true color (from CIELab color space) is displayed at the top of each diagram. Following the "path" that color takes as phaser thickness increases on the chromaticity diagram, the corresponding true CIELab color at each point $*$ is reproduced in the individual panels at the top of the diagram. Comparing (a) and (b), we can see that the path that color takes differs significantly before and after the reaction occurs. The point $*$ corresponding with the greatest distance between the paths is colored red, and it is this point which constitutes the greatest color-change for this particular set of parameters.

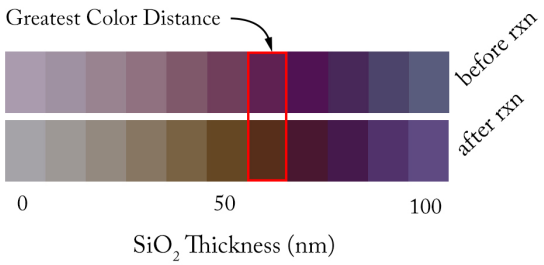

Figure 2.6: True colors produced by holding absorber thickness at 25nm, and varying resonating phaser (SiO_2) thickness from 0 to 100 nm, as in Figure 2.5. The red box indicates maximum color change between the two reaction stages (60nm SiO_2), as determined by Equation (2.4) for color distance.

Looking closer at the true colors produced by varying the thickness of the SiO_2 before and after the reaction (Fig. 2.6), we see that for $t_{abs} = 25$nm, the maximum color change occurs when $t_{phaser} = 60$nm, as determined through Eq. (2.4). Qualitatively, the color change also appears minimal without a phaser layer ($t_{phaser} = 0$nm), but grows into a more noticeable change t_{phaser} increases.

2.2.3 Visual Colorimetric Sensor Simulations

In simulations, we allowed the thickness of a phaser layer to vary from 0-400nm for each thickness of the absorber (PAR) layer, from 0-500nm. The thicknesses were taken at intervals of 5nm, giving a resolution in results fine enough to determine what the optimal dimensions of the material would be, but simulating large enough ranges to see large-scale trends in the results. The PAR absorber layer served as a representative model for a colorimetric color-change material through chemical coloration. The PAR's chemical coloration does not produce a particularly pronounced or visually impressive color-change—but its properties make it an easy and safe material to use in the laboratory for exploration of a color-changing structure.

The first structure studied was PAR-SiO_2-Si. Figure 2.7 shows the true colors of the colorimetric sensing material with ranges of thicknesses t_{abs} and t_{phaser}, before and after the reaction with Cu(II) takes place. The simulated colors show the visual appearance of the material before and after the reaction, giving us a qualitative measurement of our perception of color changes at specific absorber and phaser thicknesses. For example, at $t_{abs} = 50$nm, $t_{phaser} = 200$nm, the color of the material is light purple before the reaction, and yellow after the reaction takes place. We can observe visual color changes in this way.

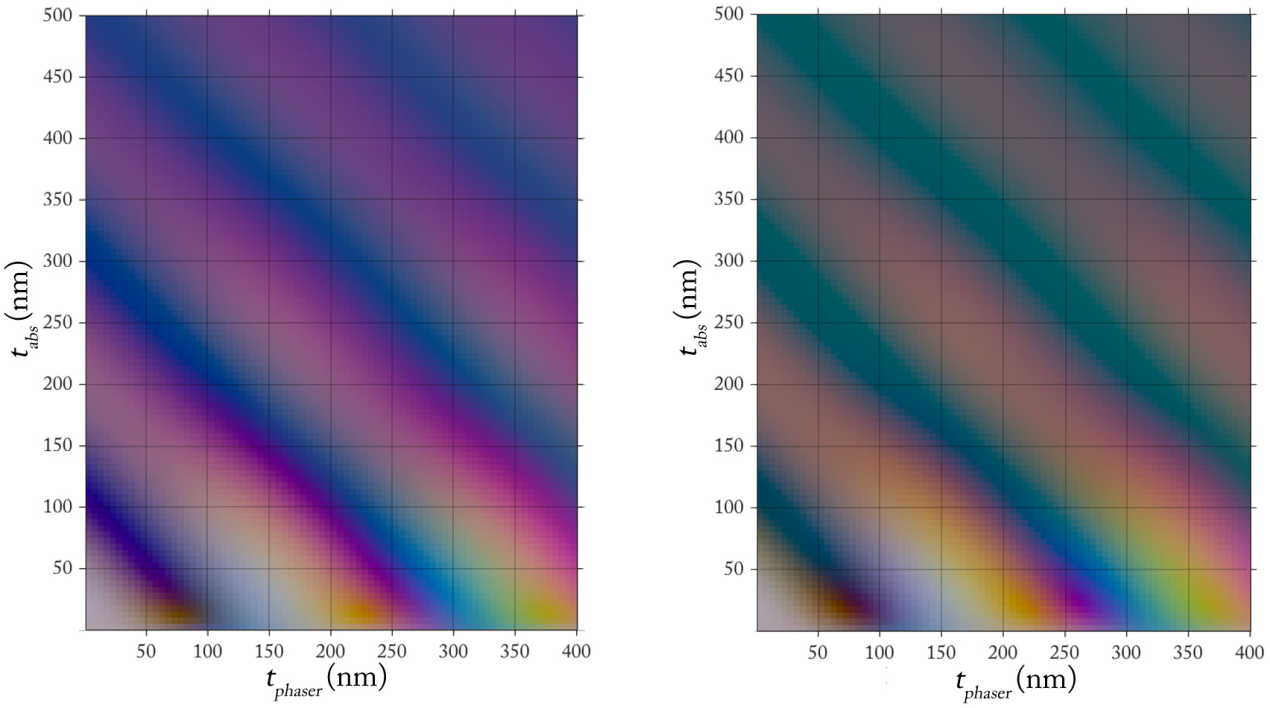

(a) Before Reaction

(b) After Reaction

Figure 2.7: PAR-SiO_2-Si Color Change. These diagrams show the expected color of the model colorimetric sensing material with a silicon substrate before (a) and after (b) a complexation reaction of the Cu(II) ions, for a range of thicknesses t_{abs} and t_{phaser}. The colors displayed are the expected color of the material for each pair of physical dimensions.

Alternatively, we can use quantitative methods established in the previous sections to assess the color change amplitude in Figure 2.7. The first quantitative method is the determination of d, the color difference, for each structure (Figure 2.8a). This provides a magnitude of the change in color, allowing us to "measure" the perceived *change* at the surface of the colorimetric material, without regard to the visual color before and after the reaction. The second method is the determination of A, the amplitude of the color change for each phaser thickness, compared to the color change without the presence of the phaser layer (Figure 2.8b). This allows us to directly compare the color change for a structure with a phaser layer of thickness t_{phaser} to the same structure without a phaser.

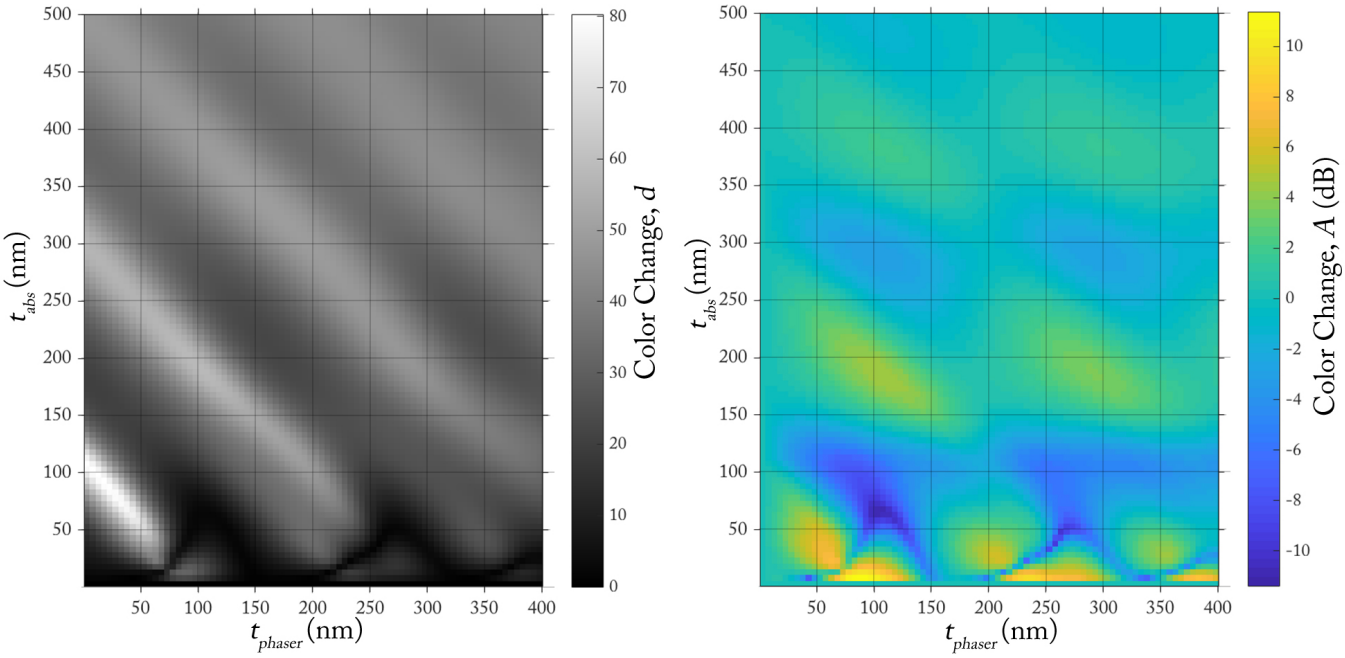

(a) Color Difference

(b) Color Amplification

Figure 2.8: PAR-SiO_2-Si Color Difference (a) is a quantitative metric that corresponds with the perceptible change in the material's color. Greater color change is indicated by higher color difference (white). Color Amplification (b) shows the isolated color difference amplification effect of adding a phaser layer to an absorber layer of thickness t_{abs}. The amplification (Eq. (2.5)) compares a physical dimension coordinate pair (t_{abs}, t_{phaser}) to a reference coordinate of $t_{phaser} = 0$. Positive amplification indicates an increase in color difference (yellow) while negative amplification indicates a decrease (blue). See Fig. 2.2 for visualization of material structures.

The same color change visualization is applied to a different structure: the same PAR absorber layer on a SiO_2 phaser, but this time, with an aluminum substrate (Figs. 2.9 and 2.10). The appearance of brighter colors in Fig. 2.9 is confirmed by the mean lightness (CIELab coordinate L) over all simulated structures. The mean lightness for structures with a Si substrate is $L = 37$ before the reaction and $L = 40$ after, while the mean lightness for structures with an Al substrate is $L = 60$ both before and after the reaction.

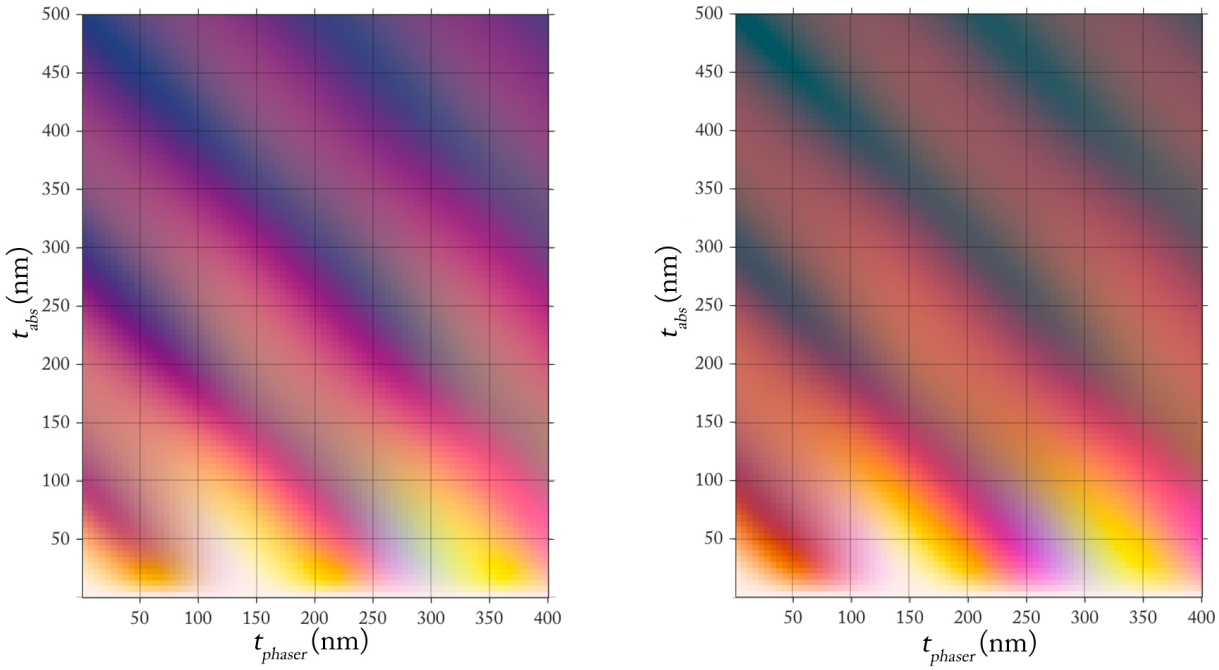

(a) Before Reaction

(b) After Reaction

Figure 2.9: PAR-SiO_2-Al Color Change. These diagrams show the observable color of the colorimetric material with an Al substrate before (a) and after (b) a complexation reaction of the Cu(II) ions with the PAR absorber layer.

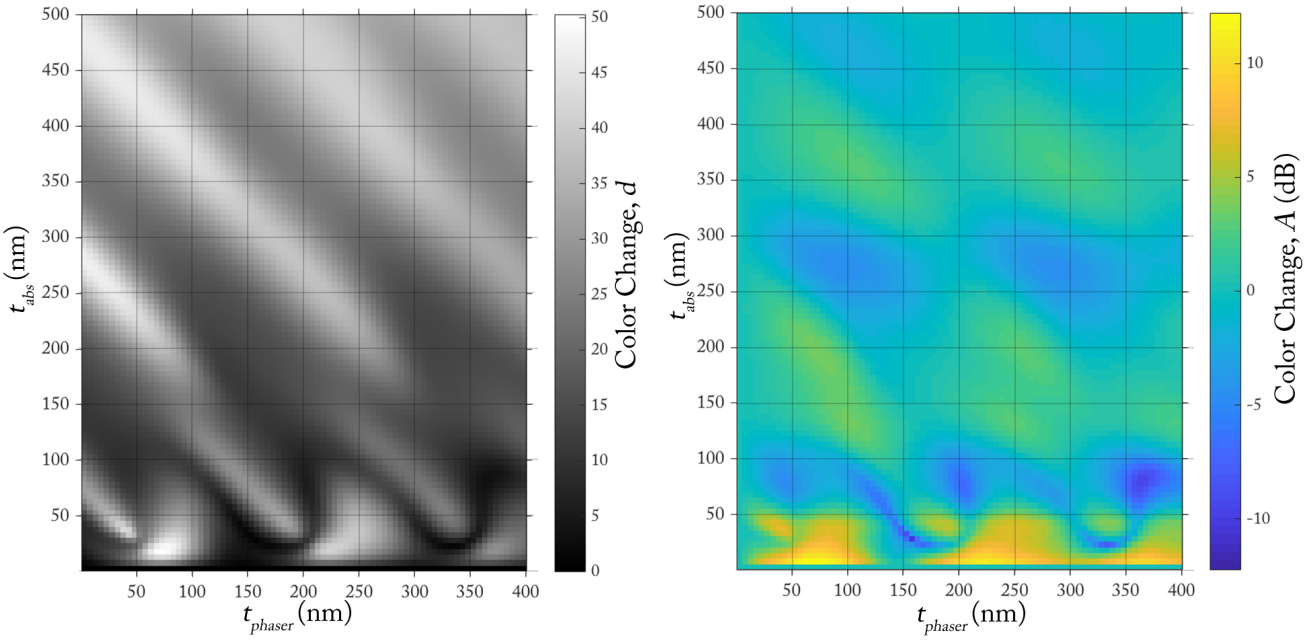

(a) Color Difference

(b) Color Amplification

Figure 2.10: PAR-SiO_2-Al Color Difference (a) and Amplification (b). Note that the color scales for both figures have been adjusted from Fig. 2.8, as the magnitude of the maximum color differences is smaller than it is for a Si substrate structure.

Brighter colors do not necessarily yield a stronger color-change, however. Comparing the color changes in the two different materials simulated, we identify the following points of maximum color change:

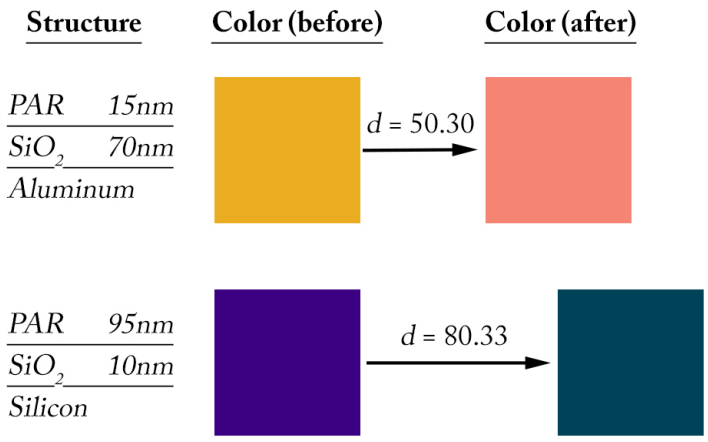

Figure 2.11: Structures of Greatest Color Difference. For each of the absorber-phaser-substrate materials, a different structure of greatest color difference exists. These structures are represented here, with their true colors and the CIELab distance d between the colors also highlighted.

The greatest color change, according to the CIELab color difference (d), is the change that takes place in the PAR-SiO_2-Si structure, with dimensions t_{abs} = 95nm, t_{phaser} = 10nm.

However, it can also be instructive to determine the effectiveness of the phaser in amplifying color change. From Eq. (2.5) and the Figures 2.8b and 2.10b, we can find the points of maximum color amplification in the structures. These points correspond with the thicknesses of t_{abs} that would most benefit from the addition of a phaser layer, and also give the thickness of that optimal phaser.

Table 2.1: Structures of greatest Color Difference Amplification

Material Substrate	t_{abs}**(nm)**	t_{phaser}**(nm)**	d **(without phaser)**	d **(with phaser)**	**Amplification** A **(dB)**
Silicon (Si)	5	85	1.67	22.94	+11.38
aluminum (Al)	5	70	1.63	27.12	+12.21

The structures of highest amplification are found to be similar in physical dimensions. Qualitatively, we can see in Figures 2.8b and 2.10b that the addition of a phaser

layer can be most beneficial for the thinnest absorber layer structures (5-20nm). In these cases, the magnitude of the color change is still much lower than the maximum possible color change.

2.3 Discussion

Results have shown that the color-change in a colorimetric sensing material can be strongly affected by the structure of that material. While chemical coloration and the change in the optical properties of the chemically reactive absorber layer remain the primary sources of a color-change, the physical dimensions of that absorber layer can dramatically alter the effectiveness of the absorber in inducing a large color difference, while also maximizing the response speed and detection sensitivity. Furthermore, the addition of a phaser layer can, in many cases, amplify that color difference considerably, leading to more perceptible color-change in colorimetric sensing materials.

The first and foremost factor in producing color in a material is the different dielectric layers used in that material. This may seem obvious, but the differences between Figures 2.7 and 2.9 demonstrate that even the deepest layer in the material, the substrate, has a great effect on the color produced. Particularly, the reflectivity of that substrate may influence the lightness of the colors produced at surface. Silicon has lower reflectivity than aluminum, and indeed, its mean lightness value for simulated structures was much lower than that of aluminum ($L = 37 - 40$ compared to $L = 60$). The choice of substrate can be strategic in producing a desired color at surface.

In contrast, as the thickness of the absorber layer grows, the differences between Figures 2.7 and 2.9 diminish. Comparing the uppermost portions of each figure, for those structures with the greatest absorber thicknesses, the type of substrate seems to matter less in the color produced. We can imagine that with an even thicker absorber layer, the color-change would solely depend on that layer's chemical coloration, since a thick absorber would limit light reaching lower levels, diminishing any structural coloration. If we look at color difference plots, Figs. 2.8a and 2.10a, we can see that the effect of increasing t_{abs} is the "graying" of those color differences. In other words, the color difference d becomes more uniform, which we would expect from a colorimetric sensor unaffected by structural coloration. Thus, we can say that in the large t_{abs} limit, the system corresponds to that of purely chemical coloration. For the purposes of comparing coloration, it may serve a good "control".

Without the effect of a phaser ($t_{phaser} = 0$nm in all figures), we see that not only the observable color but also the color difference d is affected by the absorber thickness t_{abs}. In the development of colorimetric sensing systems, the thickness of the chemically reactive absorber layer is important to consider for its effect on light phase and color-change amplitude. These effects of structural coloration on the absorber layer influence

the performance of the device and cannot be ignored, even in cases where the structure does not include a phaser layer.

Looking at the Color Difference figures 2.8a and 2.10a, it is also obvious that the Fabry-Perot cavity structure can influence the magnitude of a color-change (or color distance d). We have already acknowledged that structure plays an important role in determining both observable color and color difference d, but these figures, along with Figure 2.11, show that the inclusion of a phaser layer in that structure can be beneficial in the design of a visual colorimetric sensor. For each set of materials tested for its capacity as a sensor system, the structure of greatest color difference included a phaser.

Not only the phaser thickness t_{phaser} affects the structural coloration, however. The existence of structures with large color change for high t_{abs} and low t_{phaser} hints that the two layers may work together to produce some interference. While we might have expected vertical color modes in Figs. 2.7 and 2.9 corresponding with specific phaser structures, we instead see that the combination of the phaser and absorber layers is what produces this structural color. Recognizing this, we should make sure to include the absorer layer in our analysis of interference-based structural coloration. What's more, in the silicon substrate, the high absorption of silicon can actually serve to extend the Fabry-Perot cavity *into* the substrate. We may see this in Figure 2.11, where the structure of greatest color change has a relatively thin phaser layer, but with the Silicon substrate, the opportunity for resonance within the substrate itself. This further complicates the origin of structural coloration in the material.

To deepen our understanding of resonance's role in structurally enhanced color difference, it is helpful to look at the Color Difference Amplification (Figs. 2.8b and 2.10b). These figures directly compare the color difference of a structure with a phaser to that same structure without, eliminating the absorber thickness in determining the effect of a phaser. It is evident from these figures that a phaser may be of great utility when it comes to producing a large color change in a colorimetric sensing material. Amplification of color difference peaks at +11.38dB ($t_{phaser} = 85$nm) for a silicon substrate structure and +12.21dB ($t_{phaser} = 70$nm) for an aluminum substrate structure. Both of these peaks occur when $t_{abs} = 5$nm. This seems to roughly correspond with our expectations for a Fabry-Perot optical resonator structure. If the maximum color change occurs in the blue wavelengths, then suppression of higher wavelengths through destructive interference is desired for observable color-change amplification. If we attempt to reduce the spectral reflectance at 500nm, then we want a resonating cavity (the phaser layer) of 84nm (quarter wave thickness with refractive index of SiO_2 $n = 1.48$ at 500nm). Needless to say, the 5nm absorber layer thickness itself is significant in both maximizing response speed and detection sensivity—an original intent that motivated this exploration.

Regardless of the sources of the amplification (sources which became convolved with

the optimization of human perception of color-change), the simulations show that there is a clear benefit in the addition of a phaser, especially at lower t_{abs}. While some thicknesses t_{abs} are benefited greatly by the addition of a phaser, others are negatively affected. For example, in Figure 2.8b, we can see that potential for amplification is high for t_{abs} less than 50nm, between 150 and 250nm, and between 350 and 450nm. In contrast, the structure performs better without a phaser layer for t_{abs} roughly between 50 and 150nm, and between 250 and 350nm. A similar effect is visible for the aluminum substrate structure. The complexities of the structure and all of its optical properties can obscure the delineation of contributing factors such as the complex-valued substrate optical properties, but fortunately, the TMM simulations can account for their existence and predict their holistic effect for us. In this way, the TMM proves to be a powerful tool in identifying non-trivial structures with high color difference and/or color difference amplification.

A thin absorber layer is ideal for a number of reasons, and we have shown that in the case of these two material structures, a thin absorber layer ($t_{abs} \leq 50$nm) with a phaser layer has great potential for amplification. If such a property is exhibited in other material structures, it may prove valuable to the development of colorimetric sensing technology. A thin absorber layer can facilitate mass transport from the environment into the absorber layer. This makes the optical response to chemical stimuli faster, reducing reaction times. With that, the sensitivity of the material can also increase, leading to lower detection limits. However, the balance between optical response of the sensor and the optimal physical dimensions may both need to inform design of real sensors. Although amplification is highest when $t_{abs} = 5$nm, color difference d is much higher with other physical dimensions. For the structure with an aluminum substrate, dimensions of $t_{abs} = 15$nm, $t_{phaser} = 70$nm may prove to be a better design choice despite a lower color difference amplification (+9.4dB vs. +12.21dB) because its color difference is very high ($d = 50.30$ vs. $d = 27.12$).

In general, the methods of analysis give flexibility in the design of colorimetric sensing systems. The gamut of colors produced in Figures 2.7 and 2.9 show that with design, even the observable colors visible before and after the reaction with PAR can be controlled through structure.

In this test of the TMM for use in optimizing a colorimetric sensing structure, we have tested a representative model for a colorimetric sensing material. However, the optical constants that we assumed for the chemically reactive absorber layer (PAR) in this model were approximated from previous studies of absorption and the physical properties of sol-gel, and are not presumed to be the exact constants for the material blended with sol-gel of varying compositions. To truly gain an idea of how we should optimize this specific colorimetric sensing structure, we would need a more precise knowledge of these constants. The choice of a color-changing absorber layer can be improved for both particular applications, and for magnitude of un-enhanced color-change. The absorber

layer used here was a representative model for such a material which could be deployed, along with structural coloration enhancement, for a variety of uses. Therefore, it is the methods of simulation and analysis discussed here that are relevant and useful—their direct application to the PAR-SiO_2-Substrate structure has been hypothetical, and its results, only approximate.

Nevertheless, the exact change in complex refractive index for a reaction is not necessary to gain a more full understanding of the effect of structure—substrate type, phaser thickness, absorber thickness—on the color-change of a colorimetric sensing material, and the usefulness of the TMM in determining that change. Our optimization of the structure of a representative, model colorimetric sensing material gives us insights into the physics of interference-based structural coloration, and the color difference amplification it can induce.

Topics that remain to be explored include the use of structural coloration in improving spectroscopic colorimetry. While we have focused here on the reproduction of observable colors and visual colorimetry, the most precise colorimetric measurements come from spectroscopy. The merits of each method differ, but structural coloration may be able to improve spectroscopic colorimetry methods the same way it appears to improve visual colorimetry methods.

The use of alternative structures is another topic to be explored. While we based our assumptions of visible color change enhancement on a Fabry-Perot optical cavity model with absorber, phaser, and substrate layers, the use of different materials or different structures may further enhance observable color change. For example, the use of an additional wavelength selective absorber layer such as titanium may improve the performance of the Fabry-Perot optical cavity in producing structural color. Perhaps an alternative to the F-P structure in production of structural color would also improve visual color differences. For each alternative structure, however, the Transfer Matrix Method color simulation approach, and analysis methods used here could establish its utility.

2.4 Conclusion

In colorimetric sensing materials, an amplification in color-change is highly desirable. In order to understand the effectiveness of a color-change enhancement, it is essential to be able to quantify color and color-change. The CIELab color space offers perceptual uniformity for the quantification of color. Here, we have introduced a way to quantify color-changes via the introduction of "color-distance" and "color change amplification" in the CIELab space. With such quantifiable metrics, we can carry out designs for maximizing color-changes by physical means on top of what is achievable in chemical reactions. With physical or structural amplification of color-change, a smaller amount

of stimulus agent is needed to react with a thinner chemically-sensitive absorber layer, thereby maximizing both response speed and sensitivity (while still being always-on and zero-power).

The fundamental distinction that is emphasized throughout the methods presented here is the difference between spectroscopic colorimetry and visual colorimetry, but in fact, it is these two approaches that are bridged by the CIE-based methods for translating reflection spectra changes into visual color differences, or color-distances. The connection between reflection spectra, easily calculated using the TMM or similar computational methods, and perception of visual color opens doors to more computational approaches to visual colorimetry. With both colorimetric approaches in mind, materials can be designed for increased versatility, utility, and practicality in a number of scenarios. Sensor materials that have been extensively studied for their utility through the lens of decompositional spectroscopy can be reexamined in a new light: their utility through the lens of physiology and the human's own ability to detect spectral shifts as color-changes.

Results from reflection spectrum and observable color simulations of a representative, model colorimetric sensing material using the Transfer Matrix Method show that optimization of visual color-change is possible with the implementation of specific physical structures. The TMM is shown to be an effective method of calculating reflections of light off a multi-layered dielectric structure, and its utility is recognized through the study of reflection spectra and visual color in absorber-phaser-substrate structures.

In turn, such Fabry-Perot optical cavity structures are shown to be able to enhance the color change that would be seen at a simple absorber-substrate structure. Structural coloration, achieved with the introduction of the F-P cavity, can be used to increase the magnitude of an observable color-change by shaping the spectrum of available light for absorption in a chemically reactive absorber layer. In this way, structural coloration, a common natural phenomenon, is leveraged to increase color-changes made possible by chemical coloration effects.

In the F-P cavity structure explored here, altering the thickness of an absorber layer alone is enough to improve color difference, but in some cases, further improvements can be made with the addition of a dielectric, optically transparent phaser layer. Even the use of a specific substrate can increase the color-change at surface through reflection, and in some cases, the extension of an effective resonating cavity into the substrate layer. With the introduction of structural optimization and amplification in colorimetric sensing materials, previously identified limitations for colorimetric sensing materials—response time and detection limits, most notably—are called into question. With further exploration, many existing colorimetric sensors stand to gain from the development of structural amplification.

Ultimately, although the sources of structural and chemical sources of coloration are complex and virtually unpredictable with the use of traditional ray-optic approaches to reflection, the Transfer Matrix Method elegantly encapsulates the entire structure's photonic features in a single calculation, allowing for easy optimization of colorimetric sensing structures. Both spectroscopic and visual colorimetry stand to gain from the use of the TMM for optimization, as human physiology can be harnessed for the expansion of their uses. The increased flexibility in colorimetric material design made possible by the introduction of structurally tunable color-change amplification can lead to the expansion of the field, and improvements in current colorimetric sensing applications.

Bibliography

[1] T. Zhan, X. Shi, Y. Dai, X. Liu, and J. Zi, "Transfer matrix method for optics in graphene layers," vol. 1, pp. 1–8, 2012.

[2] G. Campa and S. M. Camporeale, "Application of Transfer Matrix Method in Acoustics," *Proceedings of the COMSOL Conference*, 2010.

[3] S. N. Gerges, R. Jordan, F. a. Thieme, J. L. Bento Coelho, and J. P. Arenas, "Muffler modeling by transfer matrix method and experimental verification," *Journal of the Brazilian Society of Mechanical Sciences and Engineering*, vol. 27, no. 2, 2005.

[4] D. J. Griffiths, *Introduction to Electrodynamics*. Cambridge University Press, 2017.

[5] R. Feynman, *The Feynman Lectures on Physics Vol. I: Mainly Mechanics, Radiation, and Heat*. Basic Books, 2011.

[6] C. T. Tindle, G. B. Deane, and J. C. Preisig, "Reflection of underwater sound from surface waves," *The Journal of the Acoustical Society of America*, vol. 125, no. 1, pp. 66–72, 2009.

[7] L. Feng, C. J. Musto, J. W. Kemling, S. H. Lim, W. Zhong, and K. S. Suslick, "A Colorimetric Sensor Array for Detection and Identification of Toxic Industrial Chemicals," *Analytical Chemistry*, vol. 82, no. 22, pp. 9433–9440, 2010.

[8] N. A. Rakow and K. S. Suslick, "A colorimetric sensor array for odor visualization," *Nature (London)*, vol. 406, no. 6797, pp. 710–713, 2000.

[9] V. G. Amelin, "Indicator papers in test methods of visual colorimetry," *Journal of Analytical Chemistry*, vol. 57, no. 8, pp. 733–738, 2002.

[10] A. D. Rakić, "Algorithm for the determination of intrinsic optical constants of metal films: application to aluminum," *Applied Optics*, vol. 34, no. 22, p. 4755, 1995.

[11] J. Liu and Y. Lu, "Fast colorimetric sensing of adenosine and cocaine based on a general sensor design involving aptamers and nanoparticles," *Angewandte Chemie - International Edition*, vol. 45, no. 1, pp. 90–94, 2005.

[12] L. M. Bonanno and U. A. Delouise, "Integration of a chemical-responsive hydrogel into a porous silicon photonic sensor for visual colorimetric readout," *Advanced Functional Materials*, vol. 20, no. 4, pp. 573–578, 2010.

[13] Z. Zhu, C. Wu, H. Liu, Y. Zou, X. Zhang, H. Kang, C. J. Yang, and W. Tan, "An aptamer cross-linked hydrogel as a colorimetric platform for visual detection," *Angewandte Chemie - International Edition*, vol. 49, no. 6, pp. 1052–1056, 2010.

[14] P. C. Jerónimo, A. N. Araújo, M. C. B. Montenegro, C. Pasquini, and I. M. Raimundo, "Direct determination of copper in urine using a sol-gel optical sensor coupled to a multicommutated flow system," *Analytical and Bioanalytical Chemistry*, vol. 380, no. 1, pp. 108–114, 2004.

[15] J. Courbat, M. Pascu, D. Gutmacher, D. Briand, J. Wöllenstein, U. Hoefer, K. Severin, and N. F. De Rooij, "A colorimetric CO sensor for fire detection," *Procedia Engineering*, vol. 25, pp. 1329–1332, 2011.

[16] F. J. Arregui, Y. Liu, I. R. Matias, and R. O. Claus, "Optical fiber humidity sensor using a nano Fabry-Perot cavity formed by the ionic self-assembly method," *Sensors and Actuators, B: Chemical*, vol. 59, no. 1, pp. 54–59, 1999.

[17] D. G. Stavenga, "Thin film and multilayer optics cause structural colors of many insects and birds," *Materials Today: Proceedings*, vol. 1, pp. 109–121, 2014.

[18] C. Hutchens and R. L. Waters, "Integrated circuit porphyrin-based optical fabry perot chemical sensor," 2008. US Patent 7,425,453.

[19] H. Wang and K. Q. Zhang, "Photonic crystal structures with tunable structure color as colorimetric sensors," *Sensors (Switzerland)*, vol. 13, no. 4, pp. 4192–4213, 2013.

[20] D. Oller, D. He, J. H. Kim, D. Pacifici, J. Xu, and G. E. Fernandes, "Colour gamuts arising from absorber-dielectric-metal optical resonators," *Coloration Technology*, vol. 133, no. 6, pp. 441–448, 2017.

[21] A. N. Araújo, R. C. C. Costa, and J. Alonso-Chamarro, "Colorimetric determination of copper in aqueous samples using a flow injection system with a preconcentration poly (ethylenimine) column," *Talanta*, vol. 50, pp. 337–343, 1999.

[22] T. Smith and J. Guild, "THE C.I.E Colorimetric Standards and their Use," *Transactions of the Optical Society*, vol. 33, pp. 73–127, 1931.

[23] "Cie technical report: Colorimetry," 2004.

[24] L. L. Hench and J. K. West, "The Sol-Gel Process," *Chemical Reviews*, vol. 90, no. 1, pp. 33–72, 1990.

[25] L. Gao, R. Lemarchand, and M. Lequime, "Refractive index determination of SiO2 layer in the UV/Vis/NIR range: Spectrophotometric reverse engineering on single and bi-layer designs," *Journal of the European Optical Society*, vol. 8, p. 13010, 2013.

[26] D. E. Aspnes and A. A. Studna, "Dielectric functions and optical parameters of Si, Ge, GaP, GaAs, GaSb, InP, InAs, and InSb from 1.5 to 6.0 eV," *Physical Review B*, vol. 27, no. 2, pp. 985–1009, 1983.

[27] L. R. Squire, "Fundamental neuroscience, 3rd ed," ch. Vision, Academic Press, 2008.

[28] G. Sharma and C. E. Rodríguez-Pardo, "The Dark Side of CIELAB," *Proc. SPIE 8292, Color Imaging XVII: Displaying, Processing, Hardcopy, and Applications*, vol. 8292, p. 82920D, 2012.

[29] G. Paschos, "Perceptually uniform color spaces for color texture analysis: an Eempirical evaluation," *IEEE Transactions on Image Processing*, vol. 10, no. 6, pp. 932–937, 2001.

[30] P. Pjanic and R. D. Hersch, "Specular color imaging on a metallic substrate," *Final Program and Proceedings - IS and T/SID Color Imaging Conference*, pp. 61–68, 2013.

[31] X. Wang and J. Shen, "Sol-gel derived durable antireflective coating for solar glass," *Journal of Sol-Gel Science and Technology*, vol. 53, no. 2, pp. 322–327, 2010.

Appendix A

PAR Optical Constants

We chose our absorbing, chemically reactive sensing layer to be a physical entrapment of 4-(2-pyridylazo)resorcinol (PAR) in sol-gel thin films through a base-catalyzed process. This process was studied previously, and the absorbance A was determined for the material before and after a reaction with Cu(II) ions took place. We used the following formula to calculate the extinction coefficient k from the absorbance A of the material before and after the reaction, as given in *Jerónimo et al., 2004*. [14, 21]

$$k = \frac{c * A}{4\pi f}$$

where f is the frequency, and c is the speed of light in a vacuum. The calculated extinction coefficient k, the complex portion of the refractive index used as the optical constant for PAR, before and after reaction is displayed in the graph below. In this graph, the extinction coefficient for wavelengths $\lambda = 700 - 800$ nm was extrapolated from the coefficient at 700 nm.

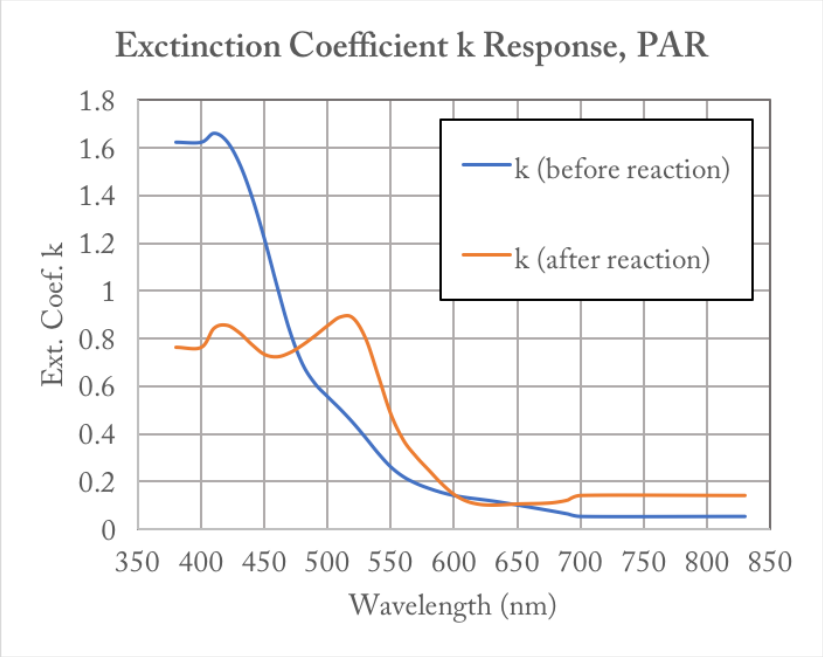

Figure A.1: Extinction Coefficient k Response. This graph shows the complex portion of the refractive index before and after reaction with Cu(II) ions. This extinction coefficient change manifests as a chemical coloration change in the absorber layer (Fig. 2.2).

Additionally, with no data given for the real part of the refractive index of the PAR material, we were forced to approximate this value from literature. It was assumed that PAR, as a sol-gel entrapment, would behave as SiO_2, because of sol-gel's noted similarity to glass. [24, 25] Thus, without any further information, we approximated this value as $n = 1.53$ for both before and after the reaction took place, for all wavelengths, a high estimate for the refractive index of SiO_2 in the optical range. A slightly high estimate for the refractive index would ensure its function as an interface for a Fabry-Perot optical cavity, the structure which demonstrated to produce structural coloration. The bounding layers of a Fabry-Perot optical cavity must have a higher refractive index than the phaser layer, so as to produce a phase shift upon reflection.

In future work, the precise refractive index of PAR will need to be determined through ellipsometry, but because of a lack of resources and difficulty preparing samples, these measurements were unavailable at the time of writing. However, the approximation of the refractive index of PAR does not hinder its ability to serve as a representative model for a colorimetric sensing, chemically reactive layer. While in simulations, the PAR optical constants were approximated for the purposes of demonstrating capability of structural coloration to enhance color-change, in future studies on colorimetric materials, a measured refractive index will produce results which can be used to optimize structure.

Appendix B

Matlab Codes for Transfer Matrix Method and Color Simulation

The following code was used to simulate reflection spectra of materials through the use of the Transfer Matrix Method, translate reflection spectra to visual color in the CIEXYZ color space, and determine color distance between material color before and after a reaction in the CIELab color space. The code starts with the highest-level class, **runcolortests.m**, which specifies the parameters to test, enabling the testing of many material structures in one click. The next class, **color_test.m** individual tests are run for a number of t_{phaser} thicknesses, and a single t_{abs} thickness. It takes CIEXYZ coordinates from the final class, and translates them to CIELab coordinates. It also writes all the data from simulations to .csv files, where the data is saved. The final class, **TMMsimulation.m**, uses the TMM to calculate reflectance spectra for individual dielectric stack structures, and translates that reflectance spectra into CIEXYZ color.

```
% runcolortests.m

% Script to run many color tests in one command. Just specify the layers,
% thicknesses, and what the index of the resonator layer is.



%% SAMPLE TEST
% seriesname = 'Si_Al_SiO2_Ti_PAR';
% layers_beforerxn = {'PAR.csv','Ti.csv','SiO2.csv','Al.csv','Si.csv'};
% t = [0,5,0,100,10000];
%
% color_test(seriesname, layers_beforerxn,3,t);


%%  TEST
layers_beforerxn = {'PAR.csv','Ti.csv','Al2O3.csv','Al.csv'};
t = [0,10,0,10000]; %nm
reslayer = 3; %the index of the resonator layer. The PAR layer is assumed to
be 1.

color_test(105:5:600,0:5:400,layers_beforerxn,reslayer,t,'save');
%the last paramter specifies whether the figures are saved in the permanent
%folder (save), or in a temporary folder, keeping files separate so as not to
overwrite data
```

```
function [X,Y,Z] = TMM_simulation(t, n ,plotter)
    % Function to determine reflection spectrum for an arbitrary material
    % stack. Can create reflection spectrum images (plotter), but otherwise
    % will just return the RGB values normalized for human vision
%% set up simulation
wvl = linspace(390E-9,780E-9,1001); %wavelengths to be tested

L = t*1e-9; % L becomes vector for layer thicknesses, with units meters

% this stuff is carried over from a more general transfer matrix
% scheme...ignore
optical = 'length'; %string is 'length' if using units of length for L, else,
optical units
incidentangle = 0; %degrees
polarization = 'tm';

%% find matrix elements
N = length(n(1,:))-2; % number of layers
kz = zeros(N+2,length(wvl)); %initialize k
a = zeros(1,N+2); %angle of incidence

for j = 1:length(wvl)
    for i = 1:N+2 % k changes with n, find k for every wavelength for every
layer
        if i>1
            a(j,i) = asin((n(j,i-1)/n(j,i))*sin(a(j,i-1))); %incidence angle
        else
            a(j,i) = incidentangle/180*pi();
        end
        if strcmp(polarization, 'tm')
            nT(j,i) = n(j,i)/cos(a(j,i));
        elseif strcmp(polarization, 'te')
            nT(j,i) = n(j,i)*cos(a(j,i));
        end
% kz is the term that goes in the propagation matrix
        kz(j,i) = 2*pi()/(wvl(j)/n(j,i))*cos(a(j,i));


    end
end
%% set up variables to be filled w reflection spectrum
Gamma = zeros(1,length(wvl)); %Gamma will record the spectrum
gamma = Gamma;
bound = cell(1,N+2);
prop = bound;

%% finish finding matrix elements
for i = 1:length(wvl)

    for j = 1:N+1
    p = (nT(i,j)-nT(i,j+1))/(nT(i,j)+nT(i,j+1));
    tau = 2*nT(i,j)/(nT(i,j)+nT(i,j+1));
          if strcmp(optical,'length')
              optL = L(j); % convert lengths to optical lengths
          else
              optL = L(j)*wvl(i)/n(i,j);
          end
```

```
    % boundary and propagation matrices for each layer j
    bound{j} = (1/tau)*[1,p;p,1];
    prop{j} = [exp(-1i*kz(i,j)*optL),0;0,exp(1i*kz(i,j)*optL)];

    end

    %% build transfer matrix from individual bound and prop matrices
    transfer = [1,0;0,1];
    for w = 1:N
        if w == N
         transfer = transfer * bound{w} * prop{w+1}*bound{w+1};
        else
            transfer = transfer * bound{w} * prop{w+1};
        end
    end

   %% TMM calculation
   % transfer applied to an arbitrary incidence
    E1 = transfer*[1;0]; % E1(1) = E1+   E1(2) = E1-= E1-
    gamma(i) = E1(2)/E1(1);
    Gamma(i) = abs(E1(2)/E1(1))^2; % reflection intensity is ratio squared

    % phase information, can be ignored
    theta1 = atan2(imag(E1(1)),real(E1(1)));
    theta2 = atan2(imag(E1(2)),real(E1(2)));
    phasedif(i) = (theta2-theta1);

end

%% Turn Reflection Spectrum into color information
colourfunc = csvread('observationfunctions.csv'); % color matching functions
xfunc = interp1(colourfunc(:,1)*1E-9,colourfunc(:,2),wvl);
yfunc = interp1(colourfunc(:,1)*1E-9,colourfunc(:,3),wvl);
zfunc = interp1(colourfunc(:,1)*1E-9,colourfunc(:,4),wvl);

% integrate reflection spectrum times color matching functions across wvl
X = 0;
Y = 0;
Z = 0;
k = 0;
for i = 1:length(wvl)
    X = X + Gamma(i)*xfunc(i)*0.3896; %multiply by the wvl interval (per CIE
recommendation)
    Y = Y + Gamma(i)*yfunc(i)*0.3896; %multiply by the wvl interval (per CIE
recommendation)
    Z = Z + Gamma(i)*zfunc(i)*0.3896; %multiply by the wvl interval (per CIE
recommendation)
    k = k + yfunc(i)*0.3896;
end
k = 100/k;

X = X*k/100;
Y = Y*k/100;
Z = Z*k/100;

%% plot figures

if strcmp(plotter,'plot1') % input determines whether to plot or not
```

```
        figure(1)
        subplot(1,2,1)
        plot(wvl,Gamma, 'LineWidth', 2)
        xlabel('wavelength (m)');
        ylabel('Reflectance (%)');
        ylim([0,1]);
        title('Colorimetric Device Reflectance (before rxn)');
        yyaxis right
        hold on;
        plot(wvl,xfunc,'Color','r','LineStyle','--');
        plot(wvl,zfunc,'Color','b','LineStyle','--');
        plot(wvl,yfunc,'Color','g','LineStyle','--');
        hold off;
        ylabel('Color Matching Function (CIE 1931)');
        ylim([0,2]);
        yyaxis left
elseif strcmp(plotter,'plot2')
        figure(1)
        subplot(1,2,2)
        plot(wvl,Gamma, 'LineWidth', 2)
        xlabel('wavelength (m)');
        ylabel('Reflectance (%)');
        ylim([0,1]);
        title('Colorimetric Device Reflectance (after rxn)');
        yyaxis right
        hold on;
        plot(wvl,xfunc,'Color','r','LineStyle','--');
        plot(wvl,zfunc,'Color','b','LineStyle','--');
        plot(wvl,yfunc,'Color','g','LineStyle','--');
        hold off;
        ylabel('Color Matching Function (CIE 1931)');
        ylim([0,2]);
        yyaxis left
end

end
```

```
function color_test(PAR_t, res_t, layers_beforerxn, resonator_layer,tin,save)
% run this script to test a colorimetric sensing structure before/after a
% chemical reaction takes place. the script will output images to results
% folder which contain useful information


%% specify layers//thicknesses
resonator_layer= resonator_layer+1; %considering air as the first layer

layers_afterrxn = layers_beforerxn;
layers_afterrxn{1} = 'PARCu.csv'; %create the second list of layers, with the
altered PAR

t(2:length(tin)+1) = tin;
t(1) = 1;
%% set up chromaticity plot

figure(1)
close;
img = imread('../CIExy1931.bmp');
minx = 0;
miny = 0;
maxx = .74;
maxy = .84;


%% clean up layers information
for i = 1:length(layers_beforerxn)
    layers_beforerxn(i) = strcat('../materials/',layers_beforerxn(i));
    layers_afterrxn(i) = strcat('../materials/',layers_afterrxn(i));
end

%% calculate the refractive indices of the layers
wvl = linspace(390E-9,780E-9,1001);
n = zeros(length(wvl(1,:)),length(layers_beforerxn)+1,2);

for j = [1,2]

    if j == 1
        layers = layers_beforerxn;
    else
        layers = layers_afterrxn;
    end

    % for each layer, the refractive index values need to be read in and
    % compiled into a matrix which describes the material stack
    for i = 1:length(layers)
        layers_nk(:,:) = csvread(layers{i},1,0);
        layers_nk(:,1) = layers_nk(:,1).*1e-6; %wvl is in microns
        layers_nk(:,4) = layers_nk(:,2)-(1i)*layers_nk(:,3);
        layerinfo{i} = layers_nk;
        clear layers_nk
    end

    for i = 1:length(layerinfo)
        layer = layerinfo{i};
        n_new = interp1(layer(:,1),layer(:,4),wvl);
        n(:,i+1,j) = n_new';
```

```
    end
    n(:,1,j) = 1; %air


end
assert(all(all(all(~isnan(n)))),...
    'Error: complex refractive indices do not cover wavelength range')



%% run different thicknesses
for t_PAR = PAR_t %run through PAR thicknesses
    t(2) = t_PAR; % the second thickness in the thickness vector takes t_PAR

    % set up chromaticity diagram
    figure(3);
    subplot(1,2,1)
    image([minx maxx], [miny maxy], img);
    subplot(1,2,2)
    image([minx maxx], [miny maxy], img);

    % run different resonator thicknesses for each PAR thickness
    resonator_t = res_t;
    structuredata = zeros(length(resonator_t),length(layers_beforerxn)+13);
    for i = 1:length(resonator_t)
        t(resonator_layer) = resonator_t(i);

        % get RGB values (normalized by color matching functions) as XYZ
        [X1,Y1,Z1]=TMM_simulation(t,n(:,:,1),''); % before rxn
        [X2,Y2,Z2]=TMM_simulation(t,n(:,:,2),''); % after rxn
        % translate into CIELab coordinates using Image Processing Toolbox
        % functions
        Lab1 = xyz2lab([X1,Y1,Z1]);
        L1 = Lab1(1);
        a1 = Lab1(2);
        b1 = Lab1(3);
        Lab2 = xyz2lab([X2,Y2,Z2]);
        L2 = Lab2(1);
        a2 = Lab2(2);
        b2 = Lab2(3);
        RGB1 = xyz2rgb([X1,Y1,Z1]);
        R1 = RGB1(1);
        G1 = RGB1(2);
        B1 = RGB1(3);
        RGB2 = xyz2rgb([X2,Y2,Z2]);
        R2 = RGB2(1);
        G2 = RGB2(2);
        B2 = RGB2(3);

        % get xy coordinates for plotting on chromaticity diagram
        x1 = X1/(X1+Y1+Z1);
        y1 = Y1/(X1+Y1+Z1);
        x2 = X2/(X2+Y2+Z2);
        y2 = Y2/(X2+Y2+Z2);

        % plot the points on the chromaticity diagrams for before/after rxn
        figure(3)
```

```
        subplot(1,2,1)
        hold on;
        scatter(x1,y1,[],'k','*');
        subplot(1,2,2)
        hold on;
        scatter(x2,y2,[],'k','*');
        dist(i) = sqrt((L2-L1)^2+(a2-a1)^2+(b2-b1)^2); %find distance
        % record coordinates and distance in matrix for later analysis
        structuredata(i,1:length(t)-1) = t(2:end);
        structuredata(i,length(t):length(structuredata(1,:))) =
[L1,a1,b1,L2,a2,b2,R1,G1,B1,R2,G2,B2,dist(i)];
    end

    %% make figures, find best distance, record data
    % determine the best resonator thickness for this specific PAR thickness
    best_resonator_t=resonator_t(dist==max(dist));
    bestdist=max(dist);
    % create the figure for the reflection spectra
    figure(1)
    set(gcf, 'Position', [100, 500, 1000, 500])
    if max(best_resonator_t)~=min(best_resonator_t)
        best_resonator_t = [best_resonator_t(1)];
    end
    t(resonator_layer) = best_resonator_t;
    %rerun simulation for the best thickness to record reflection spectrum
    [X1,Y1,Z1]=TMM_simulation(t,n(:,:,1),'plot1'); %this time, plot1
indicates to plot on the left subplot
    [X2,Y2,Z2]=TMM_simulation(t,n(:,:,2),'plot2'); %plot2...right subplot
    %determine x and y coordinates for making a red * for the point of max
    %color change
    x1 = X1/(X1+Y1+Z1);
    y1 = Y1/(X1+Y1+Z1);
    x2 = X2/(X2+Y2+Z2);
    y2 = Y2/(X2+Y2+Z2);
    % go back to the chromaticity figure and add a red point for the best
    % thickness, along with the coordinates of the best thickness
    figure(3)
    set(gcf, 'Position', [200, 700, 1000, 500])
    message = sprintf(strcat('PAR thickness = ',num2str(t(2)))...
        ,'nm // res thickness = '...
        ,num2str(t(resonator_layer)),'nm \n coldist = ',num2str(bestdist)));
    text(0.5, 0.02, message, ...
      'VerticalAlignment', 'bottom', ...
      'HorizontalAlignment', 'center','BackgroundColor','y');
    subplot(1,2,1)
    set(gca,'Ydir','Normal')
    scatter(.333,.333);
    scatter(x1,y1,[],'r','*');
    title('Before Reaction');
    subplot(1,2,2)
    set(gca,'Ydir','Normal')
    scatter(.333,.333);
    scatter(x2,y2,[],'r','*');
    title('After Reaction');
    % write a csv file which will record all of the information in
    % structuredata
    % the outputs will either be placed in the results folder or a
    % temporary folder if the data can be overwritten by the next run
```

```
    for i = 1:length(layers_beforerxn)
    C = strsplit(layers_beforerxn{i},{'s/','.c'},'CollapseDelimiters',true);
    layername{i} = C{2};
    end
    layername = fliplr(layername);
    seriesname = strjoin(layername,'_');
    layername = fliplr(layername);
    if strcmp(save,'save')
        if exist(strcat('../results/',seriesname)) ~= 7
            mkdir(strcat('../results/',seriesname));
        end
    filename1 =...
strcat('../results/',seriesname,'/PAR',num2str(t(2)),'res',...
        num2str(best_resonator_t),'reflectance.jpg');
    filename3 =
strcat('../results/',seriesname,'/PAR',num2str(t(2)),'res',...
        num2str(best_resonator_t),'chromaticity.jpg');
    else
        if exist(strcat('../temp/',seriesname)) ~= 7
            mkdir(strcat('../temp/',seriesname));
        end


    filename1 = strcat('../temp/',seriesname,'/PAR',num2str(t(2)),'res',...
        num2str(best_resonator_t),'reflectance.jpg');
    filename3 = strcat('../temp/',seriesname,'/PAR',num2str(t(2)),'res',...
        num2str(best_resonator_t),'chromaticity.jpg');
    end
    %save figures
    saveas(1,filename1);
    saveas(3,filename3);
    figure(1)
    close;
    figure(3)
    close;
    if strcmp(save,'save')
     datafile = strcat('../results/',seriesname,'/PAR',num2str(t(2)),...
         'seriesdata.csv');
    else
        datafile = strcat('../temp/',seriesname,'/PAR',num2str(t(2)),...
         'seriesdata.csv');
    end
    % write csv file recording all data for this layer thickness combination
     fid = fopen(datafile, 'w') ;
     c = {'L(before)', 'a(before)',
'b(before)','L(after)','a(after)','b(after)',
'R(before)','G(before)','B(before)','R(after)','G(after)','B(after)','colordi
st'};
     fprintf(fid, '%s,', layername{1,1:end}) ;
     fprintf(fid, '%s,', c{1,1:end-1}) ;
     fprintf(fid, '%s\n',c{1,end});
     fclose(fid) ;
    dlmwrite(datafile,structuredata,'-append');

end

clearvars
```